2013

Analysis Of Stress Waves Generated During Normal And Oblique Impacts On Aerospace Panels

Gopal Kumaran
North Carolina Agricultural and Technical State University

Analysis of Stress Waves Generated During Normal and Oblique Impacts on Aerospace Panels

Gopal Kumaran

North Carolina A&T State University

A thesis submitted to the graduate faculty

in partial fulfillment of the requirements for the degree of

MASTER OF SCIENCE

Department: Mechanical Engineering

Major: Mechanical Engineering

Major Professor: Dr. Mannur J Sundaresan

Greensboro, North Carolina

2013

School of Graduate Studies
North Carolina Agricultural and Technical State University
This is to certify that the Master's Thesis of

Gopal Kumaran

has met the thesis requirements of
North Carolina Agricultural and Technical State University

Greensboro, North Carolina
2013

Approved by:

Dr Mannur J Sundaresan Major Professor	Dr Albert Esterlin Committee Member
Dr John P Kizito Committee Member	Dr Samuel P Owusu-Ofori Department Chair

Dr Sanjiv Sarin
Dean, The Graduate School

Biographical Sketch

Gopal Kumaran was born on 22, December 1983 in Hatton, Sri Lanka. He attended school at Highlands College, Hatton and Received his Bachelor of Science degree in Mechanical Engineering from the University of Peradeniya, Sri Lanka. He is a candidate for the Master of Science degree in Mechanical Engineering at North Carolina Agricultural and Technical University.

Acknowledgements

I would like to express my gratitude to Dr. Mannur Sundaresan for giving me this opportunity and guiding me in this research. Further, I would like to acknowledge the support of my colleagues at the ISM lab.

Table of Contents

List of Figures

List of Tables

Abstract

Foreign object impact on aircraft structures is a critical event that can affect the structural integrity and compromise the safety of the aircraft. The aerospace industry devotes a considerable amount of effort to detect impact damage. The real time impact detection and quantification system can improve safety and reduce operation cost. In order to identify the impact damage, it becomes necessary to study the impact location and force history. There are a number of studies on this topic which focus on obtaining an approximate representation of force history in damage events. However, a number of important aspects of foreign object impact including the angle of oblique impact and stress distribution at the impact site are rarely addressed in these studies. The objective of this thesis is to obtain a closer representation of the impact force history based on the Hertz contact theory and verify it experimentally through acoustic emission technique. Experiments were performed on a large Aluminum plate that was instrumented with piezoelectric acoustic emission sensors capable of detecting the shear component of the acoustic emission waves. This thesis establishes that oblique impacts produce shear horizontal components in addition to other lamb wave components. Detailed finite element analysis that includes the impact dynamics as well as the resulting wave propagation was performed. The results of this finite element analysis are compared with the experimental results.

CHAPTER 1

Introduction

Aircrafts structures are prone to impact events that can lead to damage. Boeing estimates the cost associated with Foreign Object Damage (FOD) to be around 4 billion dollars a year (Boyce, Chen, Hutchinson, & Ritchie, 2001). While the larger portion of this cost is due to the FOD in the engine parts, foreign object impacts on the structure also is an important event to be considered. The location of the impact and the magnitude of the impact force will determine the extent of damage, hence complete knowledge of the impact becomes important for monitoring the structural health. Further, in the case of composite materials the angle of impact also plays an important role in determining the extent of damage given that the angle of the impact reduces the ballistic limit of the material (Shim, Guo, & Tan, 2012).

Considerable research has been carried out on impact damage to structures, with several different objectives. Some have focused on understanding the physics of the impact between the foreign object and the aircraft panel. Others have studied damage resulting from impact, in order to predict the possible failure of the material due to impact. All these studies tend to obtain the impact force history, the contact area and in few cases the damage induced. These researchers have used experimental, analytical and numerical techniques.

Stress waves generated by impact on flat panels have been studied widely. The primary objective has been to identify the location of the impact and the impact force history, including the magnitude and distribution of force applied by the impact object on to the structure. The available literature on this indicates that the researchers have assumed mostly the impact to be a simple point contact and have not studied the features of the stress waves propagating due to the impact in detail to understand the physics of the impact.

On the other hand, some researchers have solely focused on the damaging aspects of the impact and the relationship between the impact velocity and ballistic damage and tend not to focus on the actual contact event and the mechanism of the impact.

The theoretical studies on the impact try to simplify the problem in order to obtain a closed form solution for the impact mechanism. However, no detailed study to understand the relationship between the impact mechanism and the propagation of the stress waves has been carried out.

In this thesis, an integrated approach that combines the physics of the impact with the resulting stress wave generation and propagation is explored. In addition, some approximate models are also examined. The approach adopted is as follows: Hertz contact theory was applied in order to estimate the impact load. The calculated force was then incorporated into a numerical model, as a point load, and an optimization process capable of identifying the impact force, if different components of stress wave detected from experiment are available.

In order to understand the mechanics of the impact, the actual impact event of a steel sphere impacting an aluminum plate of 1.5 mm thickness was simulated numerically and the results were analyzed. These experiments were carried out on a square aluminum plate instrumented with piezoelectric sensors. The stress waves generated due to normal and oblique impacts were recorded and analyzed. With the aid of the experimental observations, an improved numerical model was generated to obtain the impact force history.

CHAPTER 2

Literature Review

2.1 Acoustic Emission

Acoustic emission (AE) can be defined as transient stress waves in a medium due to the release of localized stress energy. The release of the energy causes stress waves to propagate through the medium. The AE waves can have a frequency range up to several MHz and can be detected by sensors attached to the structure.

These propagating waves have three basic modes namely Extensional (Symmetric - S), Flexural (Anti-symmetric -A) and Shear Horizontal (SH) mode. All of these modes have multiple harmonics with '0' being the fundamental mode that exists at all frequencies.

Various sources give rise to AE signals, including crack formation, crack growth, fretting and impact. Therefore, one of the primary interests in the field of AE based Structural Health Monitoring (SHM) is to identify the source of the AE. One of the successful approaches is classifying the AE sources based on the prominent features seen in AE signals. Further, the location of the AE source is also of interest due to the influence it has on the health of the structure. A number of studies are available on this particular area and many novel ideas have been proposed to locate the source of AE.

2.1.1 Acoustic emission source location. One of the simplest methods to locate the AE source is the triangulation method. In an isotropic medium, given the velocities of the different components of the signal are known, the location of the source can be estimated with three suitably located sensors. The time difference in the arrival time of two components provides the estimation of the distance, d_i of the source from each of the three sensors. The location of the source of acoustic emission is determined by identifying the intersection point of the three circles

of radii d_i with their center being the respective sensor locations. Applying this method to an anisotropic medium is a challenging task because the velocities depend on the direction of propagation.

Baxter (2007) adopted a slightly different approach to locate the AE source. For each pair of sensors, the difference in the time of arrival, termed delta-T, of the S_0 and A_0 mode were measured (ΔT) by performing lead break tests on the structure. With the aid of these results contour lines were generated, with each line representing a certain difference in ΔT value for each sensor pair. When an AE event occurs, the ΔT value would be calculated for at least two pairs of sensors and the corresponding contour line would be chosen. The intersecting point of the two contour lines gives the location of the source. While this method is essentially the same as the triangulation technique, this approach is somewhat more convenient for complex structures. (Baxter, Pullin, Holford, & Evans, 2007)

While the triangulation technique is straightforward and simple, it has many disadvantages. Primarily, the velocities of the different components need to be known beforehand. Further, the velocities of the components are assumed to be equal in all directions which is not the case in non-uniform plates and plates made of anisotropic media such as composite materials. Further, the time of arrival of the signal at a particular sensor is recorded when the signal crosses a certain predetermined threshold value. This can lead to errors in determining the time of arrival (TOA) because when the stress waves propagate they undergo attenuation and lose amplitude. These effects have been neglected in the traditional triangulation methods and hence they introduce inaccuracies in source location.

Various improvements to the triangulation method have been suggested to overcome these issues. Hyunjo (2000) suggests employing the wavelet transformation to the received

signal, choose a particular frequency, and with the aid of the wavelet determine the TOA of that frequency at the particular sensor. This method, while addressing the attenuation issue, also improves the calculation by considering a single frequency as different frequency components would have different velocities. (Hyunjo & Young-Su, 2000). Ciampa (2010) employed a similar method, applying the wavelet transformation to determine the TOA of the anti-symmetric mode at the sensors. In this study, 6 sensors were used, in 3 pairs, in order to form a pair of sensors to have an equal TOA value and use the Newton's method to solve the set of non-linear equations (Ciampa & Meo, 2010).

Kundu (2011) employed an optimization method for source location. This method allows one to predict the location of the AE source without prior knowledge of the velocities of the component. Therefore, this method allows the triangulation method to be employed on anisotropic media such as composite structures and stiffened panels. This research has primarily focused on locating the site of impact on the structure but has not focused on the mechanism of the impact or the features of the resulting signal. They have improved this method further.(Hajzargerbashi, Kundu, & Bland, 2011)

DiScalea (2011) et al used Macro Fiber reinforced Composite (MFC) sensors, to locate the impact site and to identify the impact force history. These sensors are essentially thin strips of PZT ceramics sandwiched between two layers of electrode material embedded in epoxy matrix. In this research, MFC rosettes formed by combining three MFC sensors were used. Due to the different orientation of each sensor in the rosette and the presence of thin long strips of PZT ceramic, the sensors have directional sensitivity to the propagating waves. With this advantage, the direction of the signal is obtained for each sensor, and with the aid of two sensors the location of the source is determined.(Howard & Francesco Lanza di, 2007)

While the above methods incorporate some mathematical analysis and/or optimization methods to locate the impact site, other researchers have taken a different approach and used training data to build a library of sensor responses corresponding to a large number of excitations at different locations on the structure. Park (2012) use a Scanning Laser Doppler Vibrometer (SLDV) to measure the response of the system at various locations for the input pulse generated by a PZT actuator. Later, the actuator starts to act as the sensor when there are acoustic emission events on the structure and record the signals. The recorded signal is then cross correlated with the library of the data and the location is obtained. Even though this method reduces the time spent on computation and data analysis, a library of signals at a large number of locations and for a large number of impulse shapes and durations have to be recorded beforehand. (Park et al., 2012)

In addition to these methods and their modifications, there have been some approaches that have brought in techniques from other fields of research to identify the acoustic emission source location. For example, Worden (2000) has used the neural networks and genetic algorithms to process and determine the AE source (Worden & Staszewski, 2000).

2.1.2 Impact force history. Obtaining the impact force history from the stress waves generated by the impact event is an inverse problem. Prior knowledge of the point of impact, the behavior of the structure as well as the impactor under impact loading and certain additional parameters are necessary to determine force history. Researchers have approached this problem using some form of iterative methods. They start with an estimated force history, computing the response of the structure for the assumed force, calculating the error between experimentally determined response and the response to assumed force history and then use an optimization method to minimize the error. In this case, the response of the structure for each updated load

curve has to be obtained. Instead of using a time consuming numerical simulations, some simpler methods have been incorporated in a few of these studies.

Discalea (2011) obtained the impact force history by using the MFC sensors by utilizing an optimization technique. In this process, the algorithm starts with an assumed force history and computes the structure's response, compares the experimentally obtained waveform and the computed one, and employs the optimization algorithm to minimize the error between the two signals. At each step the force history is updated and the structure's response for the new force is computed. This was implemented using a semi analytic finite element technique. Even though they have demonstrated the effectiveness of this method, it has been assumed that the impact results in a point contact and fails to identify important features related to the load distribution and oblique impact. (Bartoli, Salamone, Di Scalea, Rhymer, & Kim, 2011)

Hu (2007) has proposed a method employing Chebyshev polynomials to identify the force. (Hu, Fukunaga, Matsumoto, Yan, & Peng, 2007). Further, Chunlin (2010) has employed time reversal method to identify the impact force, though this has not been verified experimentally (Chunlin & Fuh-Gwo, 2010). Inoue (2001) used deconvolution to estimate impact force history (Inoue, Harrigan, & Reid, 2001).

The studies summarized above assume that the impact results in the application of force at a single point and neglect distributed forces that have both normal and in-plane components with varying time histories determined by the dynamic contact mechanisms that include elastic and inelastic deformations. While these methods are useful to locate the impact site and estimate the load history, they fail in one important aspect, i.e. without understanding the mechanism of the impact, the severity of the impact cannot be predicted accurately. There is another group of literature whose objective is to understand the local damage and penetration

from projectile impact but exclude any consideration of stress waves generated by the impact forces.

2.2 Hertzian Contact

According to classical contact mechanics, the contact between two elastic bodies occurs over an area. The bodies deform, and the amount of deformations depends on the elastic moduli of the materials in contact. Hertz theory gives the contact stress as the function of normal contact force, and geometrical and material properties of the two bodies in contact (Johnson, 1985).

Various approaches have been proposed to calculate the applied force, which in the case of impact, varies with time. According to the Hertzian contact theory, for two isotropic bodies of revolution, the contact occurs in a circular zone of radius *a* in which the normal pressure *p* varies as

$$p = p_0 \left[1 - \left(\frac{r}{a}\right)^2\right]^{\frac{1}{2}}$$

Where p_0 is the maximum contact pressure at the center of the contact zone and *r* is the radial position of the point at which the pressure *p* is being calculated. The contact force between the two bodies is defined as

$$F = k_c \alpha^{3/2}$$

Where k_c is the contact stiffness and α is the depth of indentation.

The combined modulus E*, $\frac{1}{E^*} = \frac{1-\nu_1^2}{E_1} + \frac{1-\nu_2^2}{E_2}$

And the effective radius R, $\frac{1}{R} = \frac{1}{R_1} + \frac{1}{R_2}$ and $k_c = \frac{4}{3} E\sqrt{R}$

Here the parameters R_1 and R_2 are the radii of the contacting bodies, E_1 and E_2 are the young's moduli of the corresponding materials and k_c is the contact stiffness.

The maximum contact pressure is given by

$$P_0 = \frac{3F_{max}}{2\pi a^2}$$

Where,

F_{max} – Maximum contact force

a - radius of the contact area is given by

$$a = \left(\frac{3FR}{4E}\right)^{\frac{1}{3}}$$

And the parameter α is given by

$$\alpha = \frac{a^3}{R}$$

Most of the parameters calculated above, namely a, F, p and α are time dependent, the magnitudes change over the duration of the contact (Abrate, 1998). Calculating the parameters in a complex system is a challenging task. Abrate (2001) suggests simplifying the contact as a spring mass model (Abrate, 2001). Depending on the complexity of the system and the required accuracy, it is convenient to model the system as a one, two or multiple degree of freedom system.

When modeled as a one degree of freedom system, the combined contact parameters k_c and the mass of the impactor is used to determine the displacement of the impactor i.e. the elastic indentation of the plate due to impact. While this is a gross simplification, it gives a general idea of how the impact force varies with time and lets one calculate the other parameters. However, if permanent indentation occurs during impact the contact force history will follow a different path during the unloading phase. A modified contact law was suggested by crook for the unloading phase.

$$F = F_m[(\alpha - \alpha_0)/(\alpha_m - \alpha_0)]^{2.5}$$

where F_m is the maximum contact force before unloading and α_m is the maximum depth of indentation and α_0 is the depth of the permanent indentation.

In order to obtain a more accurate force history, a two degree of freedom system was modeled and the resulting set of simultaneous differential equations is solved. This model provides a better approximation of the impact mechanism than the two degree of freedom model, but when compared to the actual impact force histories obtained by other means the results were still inaccurate. Therefore, the better alternative is to simulate the impact numerically using a Finite Element approach.

2.3 Impact Force History in Impact Damage

Batra (2012) in his analysis of failure of fiber reinforced polymeric composite determined the impact force history through numerical simulation. The features of force history were related to the damage mechanism (Batra, Gopinath, & Zheng, 2012). Setoodeh (2009) numerically simulated the impact on anisotropic material through Hertzian contact. But the study is limited to the effectiveness of the developed algorithm in measuring the impact force. (Setoodeh, Malekzadeh, & Nikbin, 2009).

Chang (2012) predicts the impact induced damage in composite structures using numerical simulation. A database of estimated damage information is created using numerical simulation and pattern recognition methods. The impact damage is estimated comparing stress waveform with the data available in the database. Even though the impact force history has been obtained in this study, the actual contact mechanism has not been considered (Roy, Mueller, Janapati, Das, & Chang, 2012). Menna (2011) in their study on delamination of composite structures due to impact, have modeled a circular plate and hemispherical impactor and have numerically simulated the impact event and obtained the force history (Menna, Asprone,

Caprino, Lopresto, & Prota, 2011). There are a number of similar studies that numerically simulate the impact and to estimate the impact force history without looking at the contact mechanism involved or the stress waves generated by the impact.

This research focuses on the stress waves generated during the normal and oblique impact while relating the features of the stress waves to the impact mechanism in order to come up with a more accurate technique to identify the impact force history.

2.4 Oblique Impact

Mindlin and Deresiewicz studied and proposed a theoretical approach to the problem of oblique contact of spheres (Mindlin & Deresiewicz, 1953). This theory was extended to analyze oblique impact by Maw et al (Maw, Barber, & Fawcett, 1976).

In this analysis, the impact forces, normal to the surface and in-plane, are analyzed separately. The normal forces are assumed to comply with the Hertz theory and the in plane loads are assumed to be independent of the normal forces. In order to obtain the time history of the loads at various points, a series solution method was proposed by Maw. The contact region was divided into 'n' circular bands and the expression for the traction (f) at each band is given as

$$\frac{(2-\nu)a}{4G}\sum_{i=1}^{n} A_{ij}f_i = u_x(j) + v_x\delta t$$

Where,

a – Maximum contact radius

G- Shear modulus of the material

u_x – Planar displacement

v_x – Instantaneous in plane velocity

Aij – Coefficient determined based on the stick – slip conditions

by solving the above equation for each time step the planar load history for the impact can be obtained. It is essential to mention that at each time step the in calculated load needs to be compared to the critical friction force and the coefficients have to be re-adjusted.

CHAPTER 3

Reverse Force Calculation

Estimation of the impact load is a widely studied problem in the field of Acoustic Emission based structural health monitoring. In practice this is a challenging inverse problem. The stress waves undergo material related attenuation and further distorted by reflections at the boundaries. Various approaches have been proposed and applied with various degrees of success. Building a library of signals generated by different kinds of loads, deconvolution method, time reversal method and optimization method are few of the widely studied ones.

The optimization method proves to be a simple and effective method. In this process, the AE signals recorded by the sensors due to an impact event are compared with the signals generated due to the application of arbitrary loads on the same structure. Using an optimization algorithm to update the arbitrary load to minimize the error between the two signals leads to the estimation of the impact load. The major disadvantage of the process is the need to obtain the signals generated for various arbitrary loads. Relying on numerical simulations becomes impractical due to the time consumed to solve each updated force. Semi Analytical Finite Element (SAFE) method was used by Bartoli et al (Bartoli et al., 2011). In this research a simpler method, impulse response function method, was employed.

3.1 Impulse Response Function

In vibration analysis, the impulse response function method is a convenient method to identify the response of a system to an arbitrary load input to the system. For a one degree of freedom system (1DOF) the response of a unit impulse load, figure 3.1, x(t) is given by

$$x(t) = \widehat{Fh(t)}$$

Where h(t) is the impulse response function.

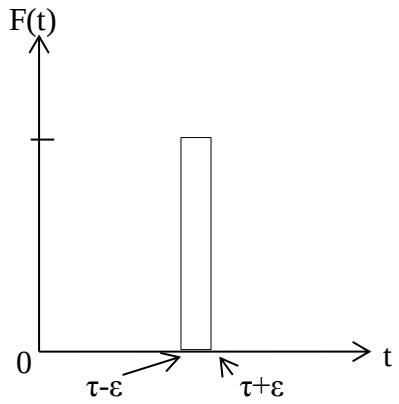

Figure 3.1. A unit impulse

For an arbitrary input function, the response of the system is calculated by means of the impulse response method. The arbitrary input is divided into infinitesimal impulses, calculate the responses to these individual impulses and add them together to calculate the response. (Figure 3.2)

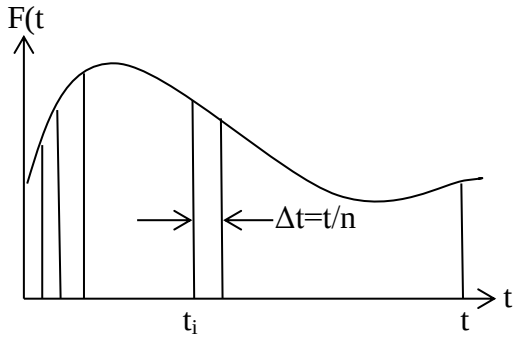

Figure 3.2. Arbitrary excitation force split up into 'n' impulses

The response of the system is given by

$$x(t) = \int_0^t F(\tau)h(t-\tau)d\tau$$

This approach is used to numerically determine the waveform generated by any arbitrary load. With this ability to generate the waveform corresponding to any arbitrary load in combination with the procedure described in the next section, it is possible to estimate the force history from an experimentally determined waveform.

3.2 Numerical Simulation

A load curve was generated according to Hertz contact theory. The calculated load was applied to the model of the plate as a point load and the stress wave was recorded at the sensor location (450 mm from the load point). The material properties used in the numerical simulation and the load curve calculation are given in Table 3.1. In these simulations it was assumed that the material does not yield, therefore linear elastic material properties were assigned to the material models.

Table 3.1

Material Properties

Material	Young's modulus/(GPa)	Density/(kgm^{-3})	Poisson's ratio
Aluminum	69	2.7	0.3
Steel	207	7.63	0.3

Figure 3.3 shows the time history of load applied at a single point and the stress waves generated due to the load. Symmetric and anti-symmetric components are easily identifiable in the waveform recorded. Further, it is observed that the reflection of the S_0 component being super imposed on the A_0 around the 200 μs mark and the reflections of the A_0 components coming in around 375 μs mark.

The load was applied normal to the surface; hence no SH component is present in the waveform obtained from this simulation. In order to reduce the computing time required to run the optimization code, it was decided to verify the results by applying a load with shorter duration. The procedure is explained in the next section.

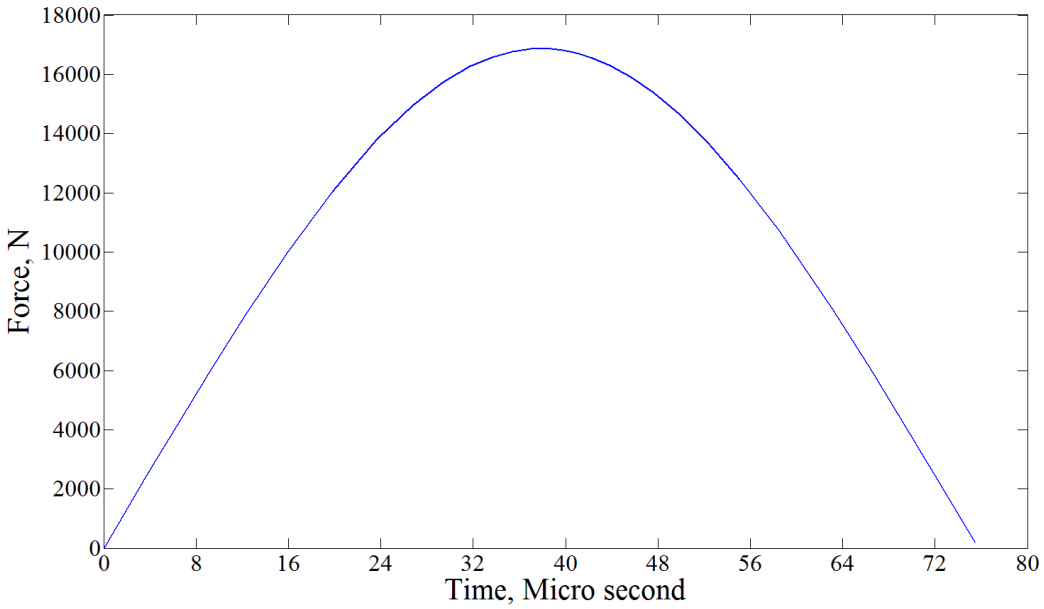

(a)

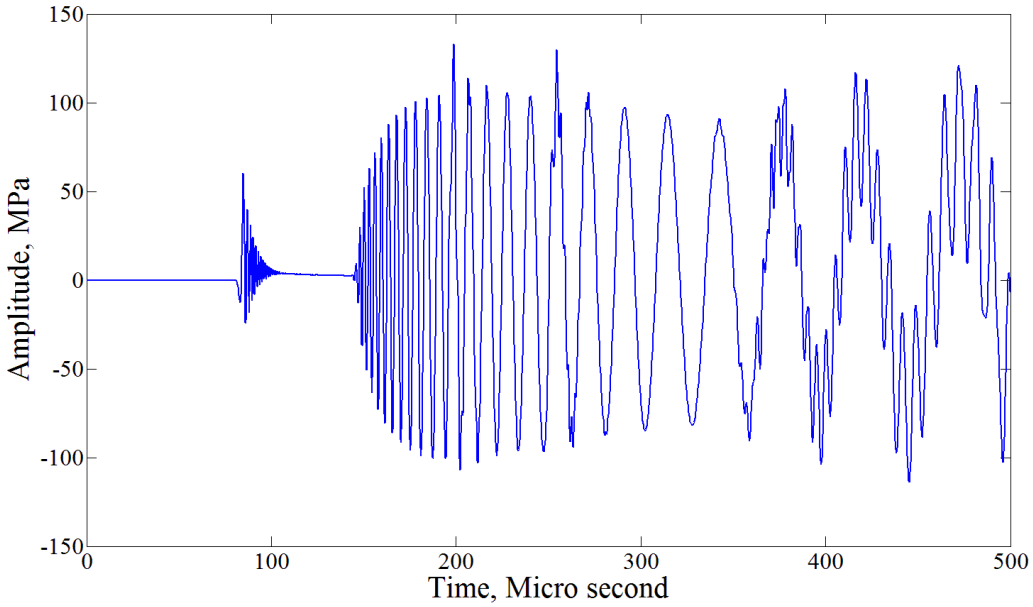

(b)

*Figure 3.3. (a)*Applied load (b) System response

3.2.1 Procedure. In order to identify the applied load, first the system response for a unit impulse was recorded by applying a unit impulse in the numerical simulation, both in-plane and

normal to the surface. Then the arbitrary load (assumed to be unknown) was applied to the same model and the response was recorded. With the assumption that the load curve is unknown (duration and amplitude) along with the angle of the impact, the process starts with an assumed load with an arbitrary impact angle and duration, obtains the stress wave by adding the response to the unit impulse with appropriate amplitudes. Then the error between the two waveforms, actual and the estimated is calculated and an optimization algorithm is employed to update the amplitudes in order to minimize the error.

Nelder-Mead simplex algorithm was used in this optimization process. The error between the actual system response and the response for the guessed force was minimized by the algorithm and the estimated load with the least error was obtained. The applied load, the response of the system for the applied load as well as the estimated load and the system response for the estimated load are given in figures 3.4, 3.5 and 3.6.

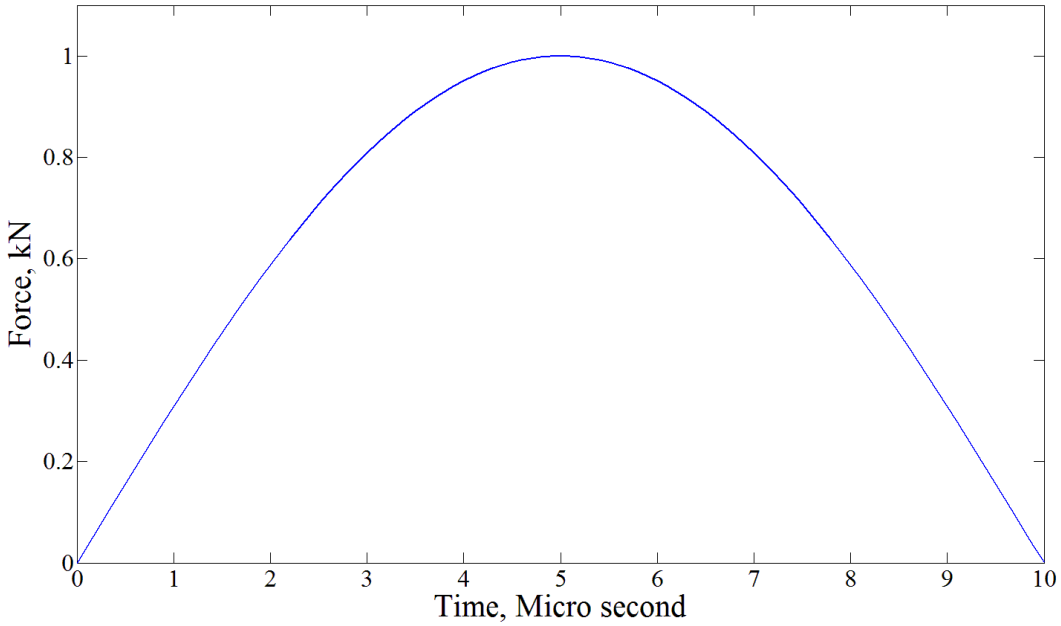

Figure 3.4. Applied load

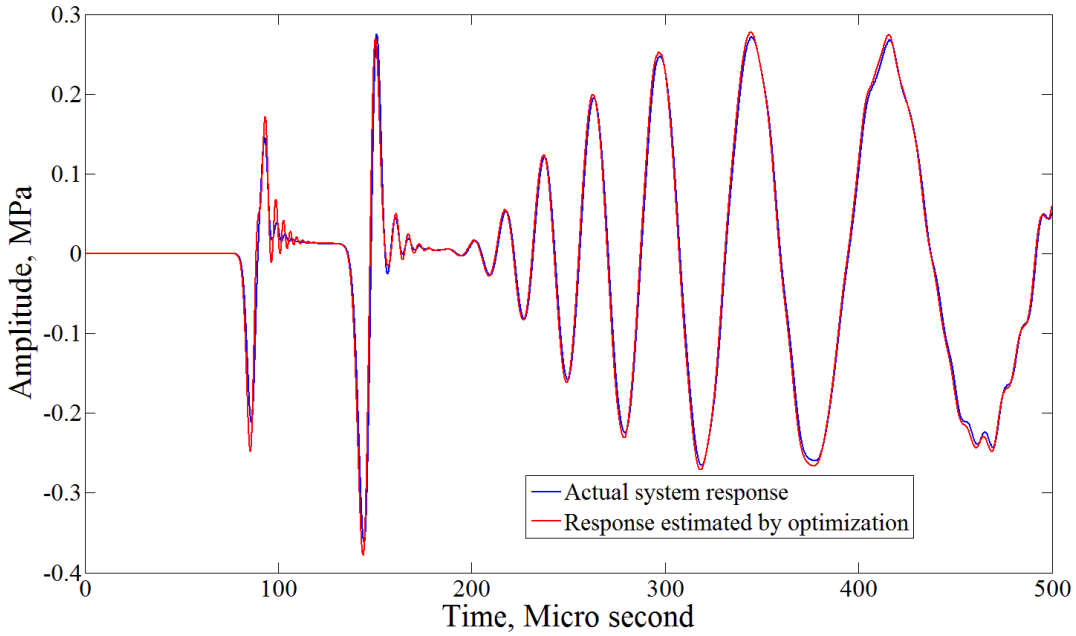

Figure 3.5. Estimated and the actual system responses

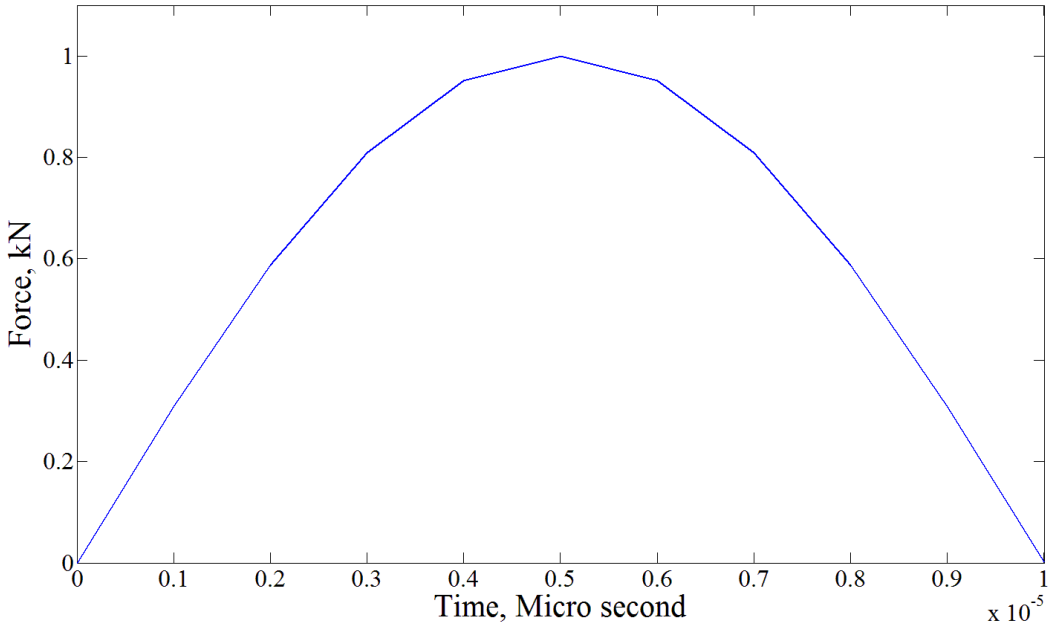

Figure 3.6. Load calculated through optimization

From the results it is obvious that the optimization program could be successfully implemented to identify the impact force when only the system response is known even though this hasn’t been demonstrated experimentally.

CHAPTER 4

Experiment

4.1 Experiment Setup

The impact experiment was carried out on an Aluminum plate of dimensions 1200 mm x 1200 mm x 1.5 mm. The plate was instrumented with the piezoelectric sensors specially designed to detect shear waves along with traditional piezoelectric wafer sensors. The sensor arrangement is shown in figure 4.1.

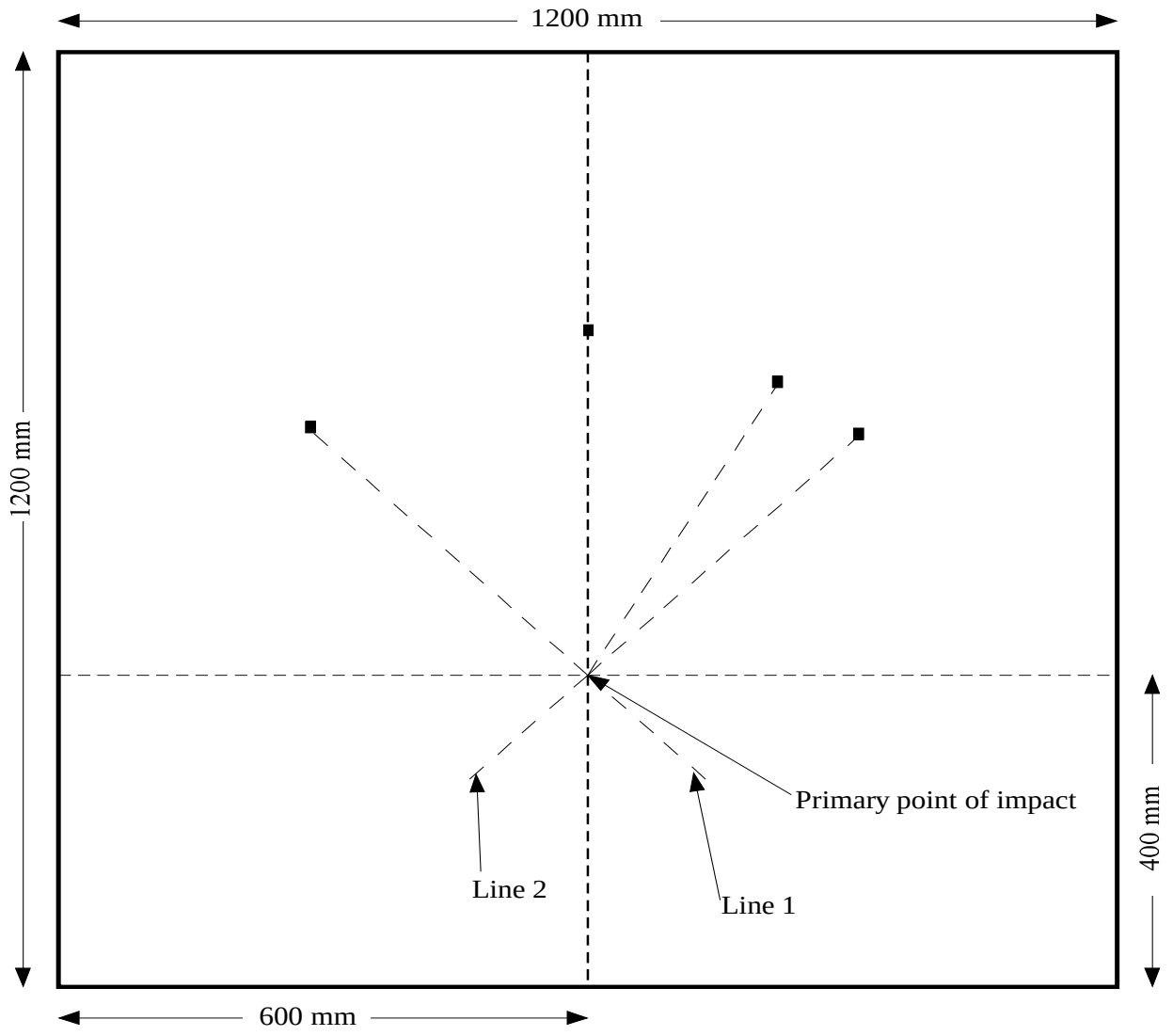

Figure 4.1. Schematic of the sensor arrangement

A 6 mm diameter steel ball bearing was used to impact the plate. An electromagnet was used to release the steel sphere from a height of 1200 mm. The experimental setup is shown in figure 4.2.

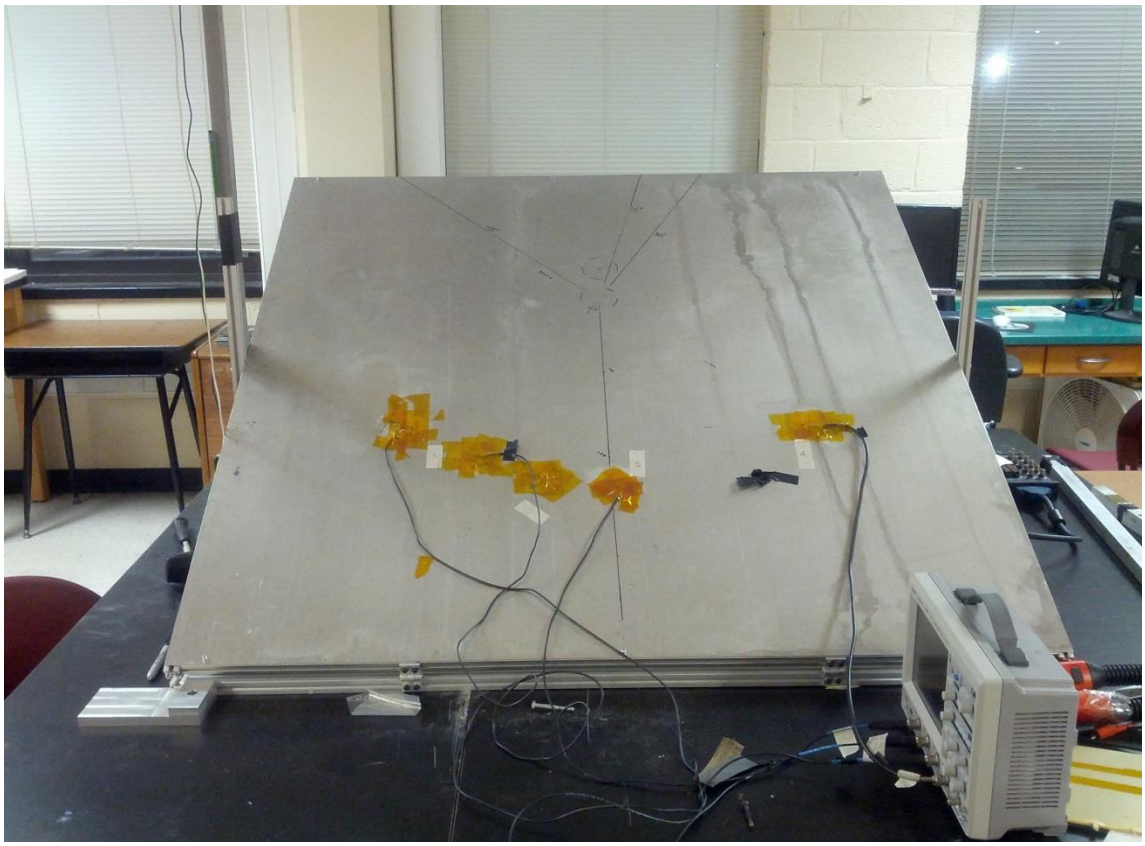

Figure 4.2. Experimental setup

4.2 Instrumentation

4.2.1 Oscilloscope. Lecroy Wavejet, model 324, oscilloscope with four input channels and a maximum sampling rate of 2 GS/s was used to record the waveforms. The oscilloscope has a 200 MHz bandwidth. After the initial observations it was evident that an oscilloscope with higher vertical resolution is necessary and Lecroy Waverunner LT344 oscilloscope with a 3 bit vertical enhancement was used in order to be able to record the waveforms without losing all the information.

4.2.2 Sensors. PZT (Lead Zirconate Titanate) ceramic sensors were bonded to the surface of the aluminum plate at the predetermined locations. The conventional rectangular sensors and the new shear sensors were both used in the experiment. (Figure 4.3)

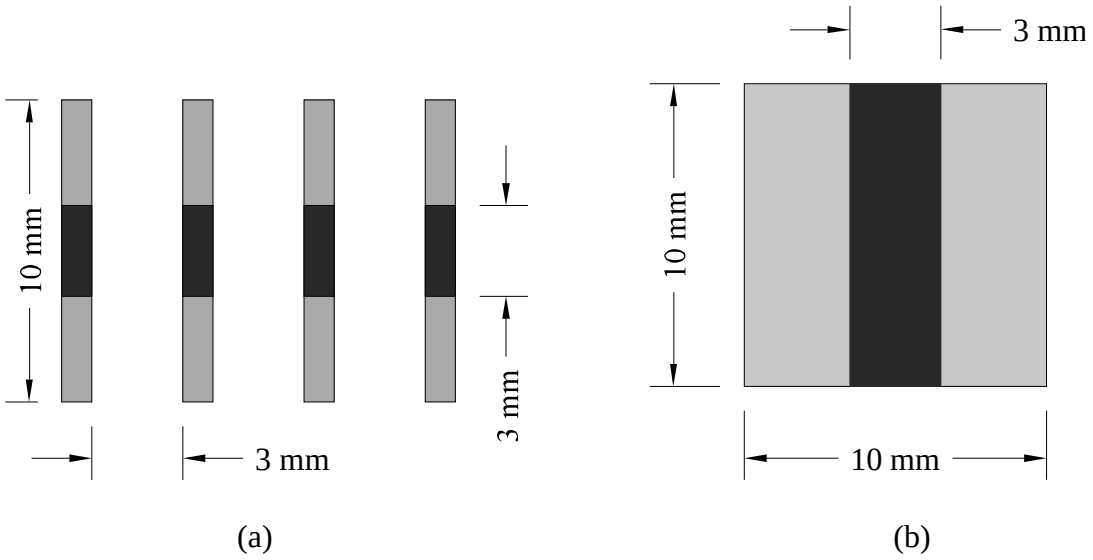

Figure 4.3. Sensor dimensions and arrangements (a) Shear sensor (b) Conventional sensor

The conventional sensors are of dimension 20x10 mm^2, and are not sensitive to the shear horizontal components of the stress waves. The new shear sensors are thin strips of dimension 20x1 mm^2 and were bonded as an array of 4 strips at each location. Each array consists of 4 strips separated by a distance of 3 mm and connected together by a thin aluminum foil. These sensors are sensitive to the shear horizontal component as well as the symmetric and anti-symmetric components.

4.3 Procedure

The sensors were connected to the oscilloscope and the oscilloscope was set to the 'single' recording mode in order to capture the waveform generated during the initial impact. To capture the symmetric, anti-symmetric and shear components of the waveforms with sufficient resolution, experiments had to be repeated with different settings for the oscilloscope. The four different settings are given in table 4.1.

Table 4.1

Oscilloscope Setup Used to Record Waveforms

	Volts per division, mV	Time per division,µs	Sampling rate, MS per second	Length of data, $x10^3$ points
Setup 1	20	50	20	10
Setup 2	200	50	20	10
Setup 3	500	50	20	10
Setup 4	1000	50	20	10

For the normal impact, an electro magnet was positioned above the point of impact at a height of 48 inches, and the steel ball bearing was released from the magnet by activating a switch. This procedure ensured that the point of impact was consistent throughout the experiment and the rotation of the sphere was very small. The recorded waveforms were saved to a memory stick from the oscilloscope for further analysis.

For the oblique impacts, the plate was raised from one end with the mechanism implemented in the fixture and set up at the desired angle and the sphere was dropped by the same procedure and the waveforms were recorded. The drop height was adjusted to compensate the change in the elevation of the point of impact caused by raising the plate.

Further, several impacts were performed at 100 mm, 200 mm and 300 mm lengths along the line 1 & 2 shown in figure 4.1 in order to gather more information about the components of the waves present in the recorded waveforms. These results were used to calculate the velocities of the components recorded by each sensor and compared with those that are available in the literature to verify the presence of each component. In addition, wavelet analysis was performed on the recorded signals.

4.4 Results

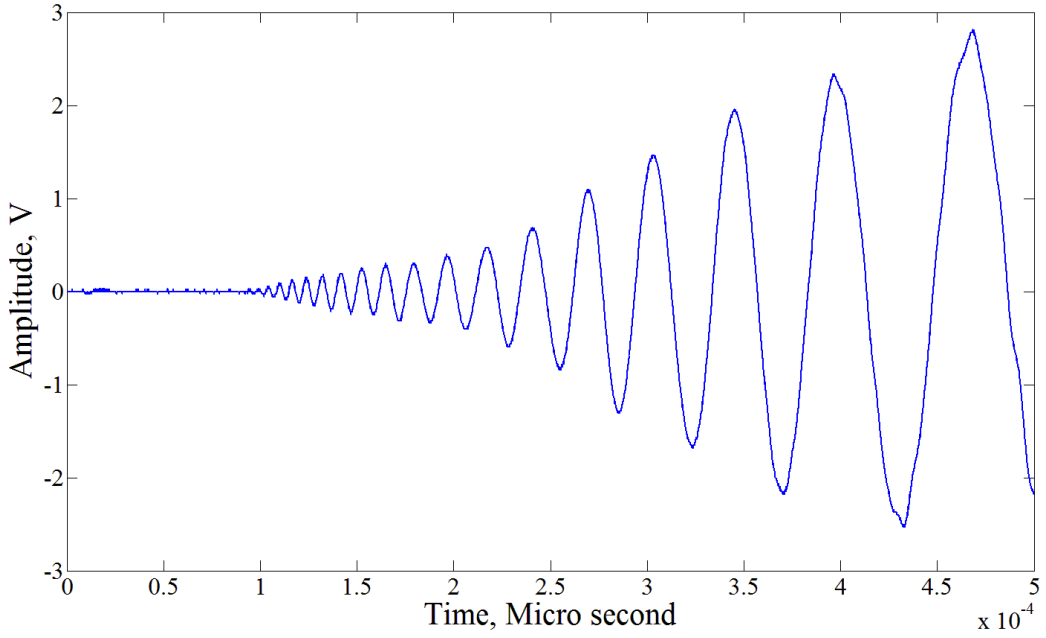

Figure 4.4. Waveforms captured for a normal impact

Figure 4.4 shows the waveform recorded for a normal impact during the experiment. Looking at figure 4.4 it is obvious that the symmetric component of the waveform has a very small magnitude compared to that of the anti-symmetric component. Therefore further experiments were carried out after increasing the sensitivity of the oscilloscope to capture the S_0 component. The magnified symmetric component of the waveform is shown in figure 4.5.

The magnified waveform shows the features of the symmetric component clearly. Further it was calculated that the ratio between the amplitudes of the symmetric and anti-symmetric components is 0.006. When compared to the point load simulations in chapter 3 (Figures 3.3 and 3.5) the S_0 component lacks higher frequency components. The anti-symmetric component consists of high frequency signals that are not present in the point load simulations. Also, the amplitude ratio of S_0/A_0 in the point load case is close to or greater than 1. Which is several orders larger than the values obtained from the experiment.

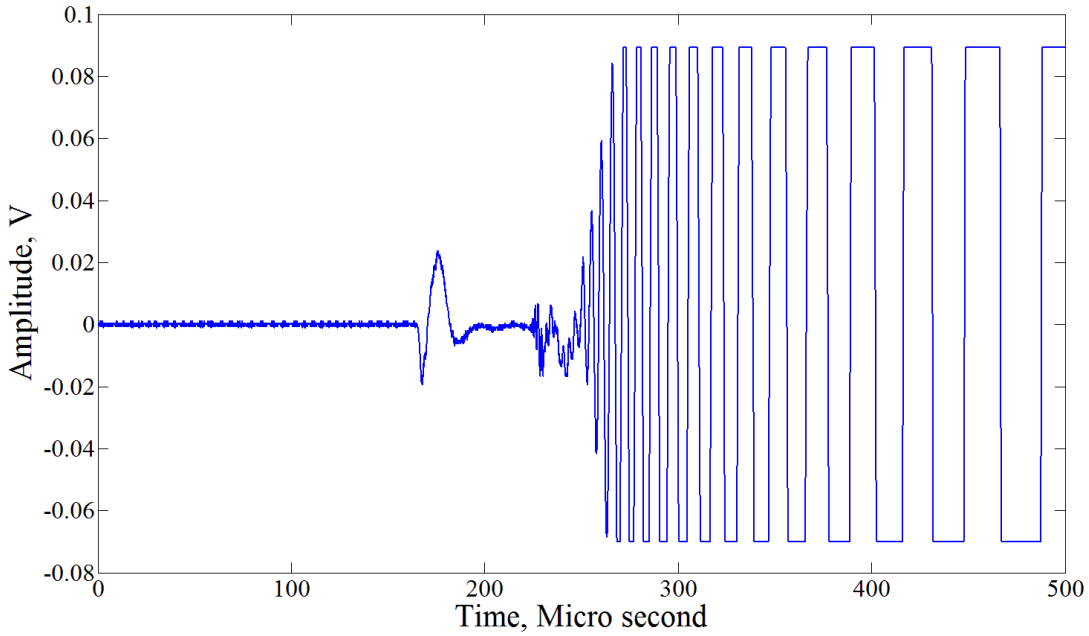

Figure 4.5. Waveforms captured for a normal impact

Additional experiments were carried out for impacts occurring at an angle to the normal axis of the plate, namely 30 degrees and 45 degrees. The waveforms clearly show the presence of the shear horizontal component. See figure 4.6.

Experiments with oblique impact angles produced amplitude ratios for both S_0/A_0 and SH/A_0 in the range 0.005-0.006. From the above observations it was concluded that the in-plane forces produced during the impact are very small compared to that of the normal loads exerted. This holds for both normal and oblique impacts. Throughout the experiment, the plate surface was inspected for permanent indentations and damage.

Further the signal recorded by the conventional wafer sensor for the same impact at 45 degree planar angle does not show the shear horizontal component; instead it shows higher sensitivity to the S_0 component. The recorded waveforms are shown in figures 4.6, 4.7, 4.8 and 4.9. As expected, the shear horizontal component shows the highest amplitude at the 45 degree propagation angle (Figures 4.6 and 4.8).

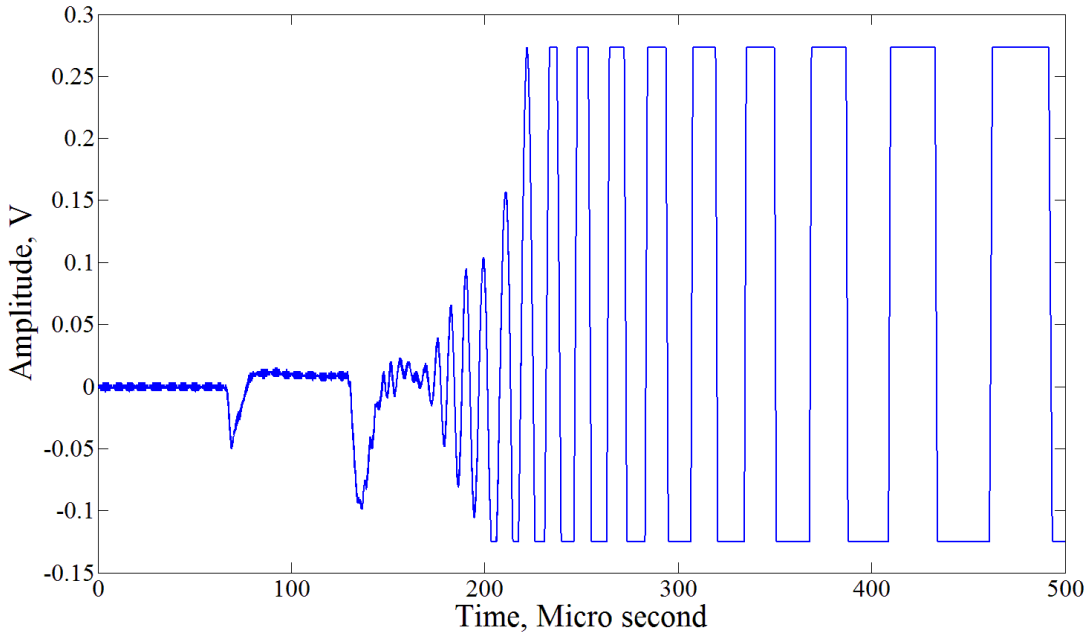

(a)

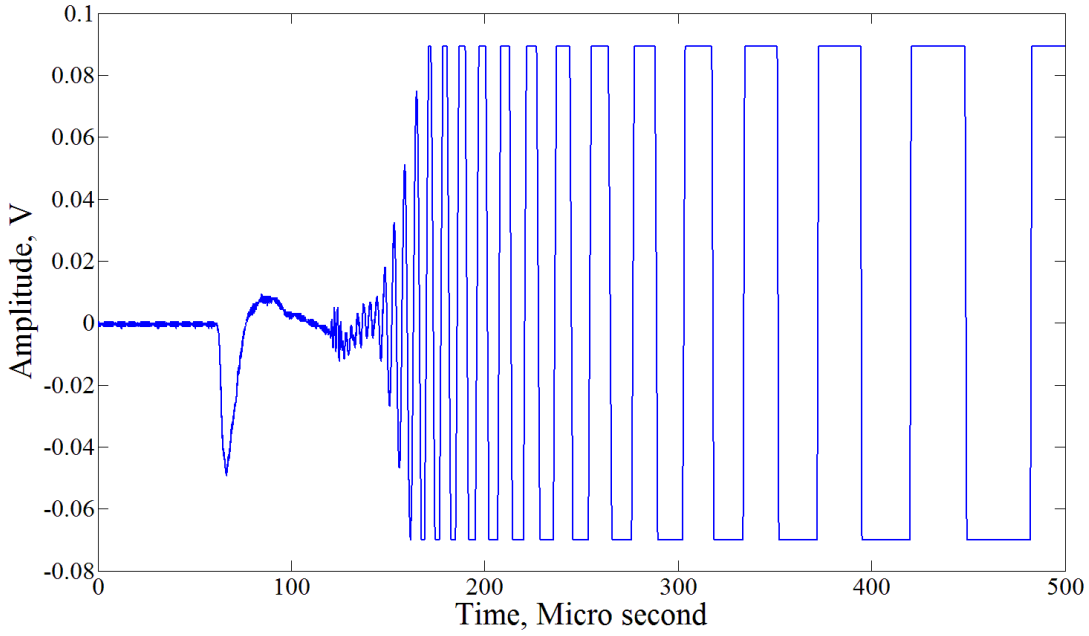

(b)

Figure 4.6. Waveforms captured by sensors for a 30 degree impact at (a) 45 degrees and (b) 0 degrees

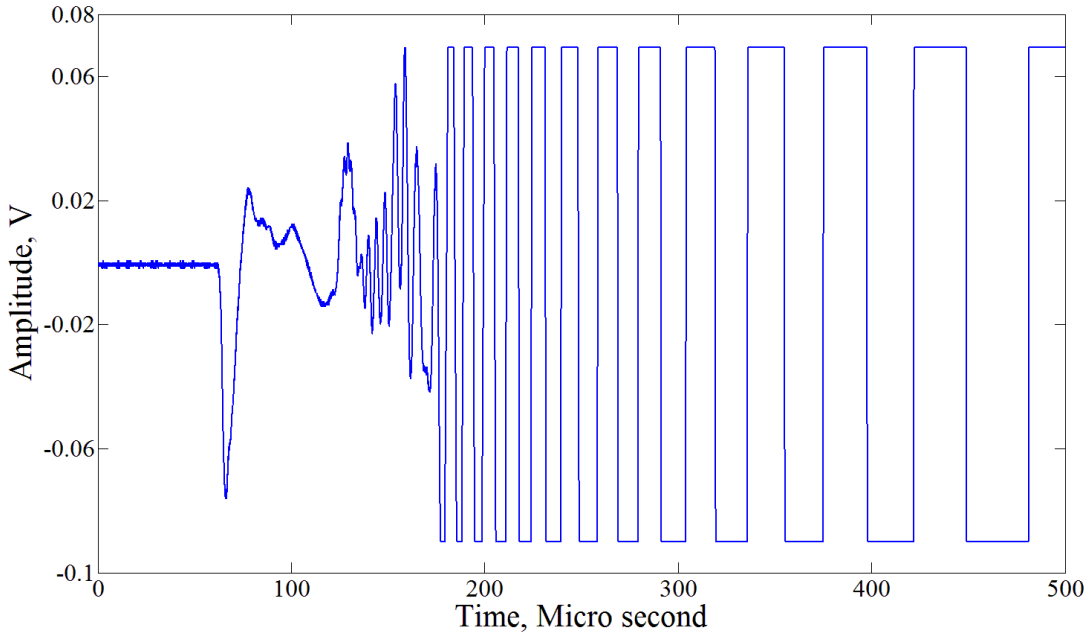

(a)

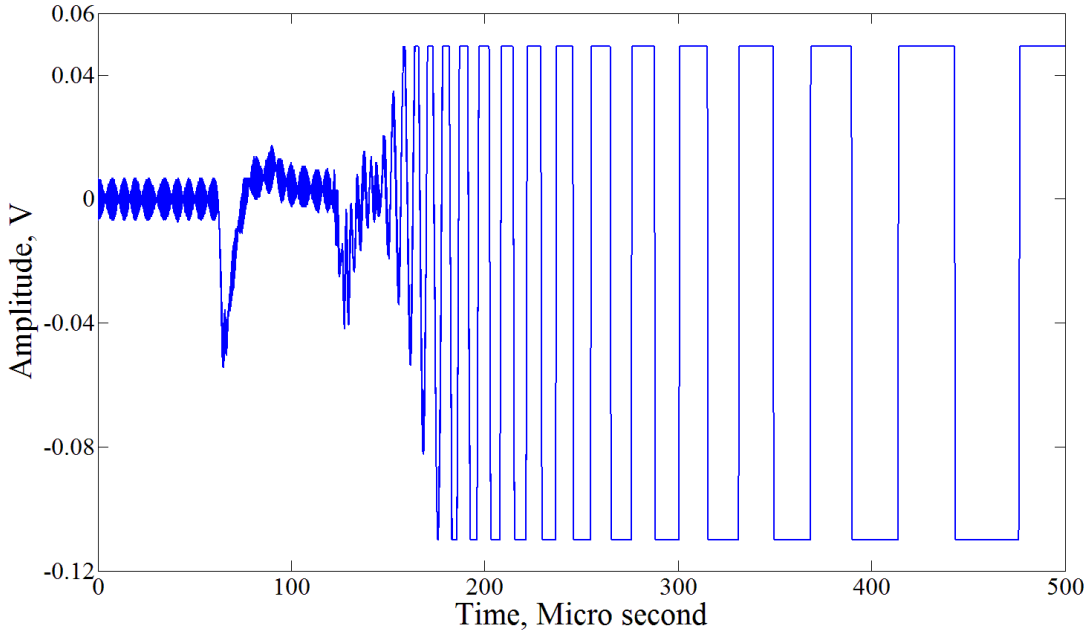

(b)

Figure 4.7. Waveforms captured by sensors for a 30 degree impact at (a) 45 degrees wafer sensor and (b) 30 degrees

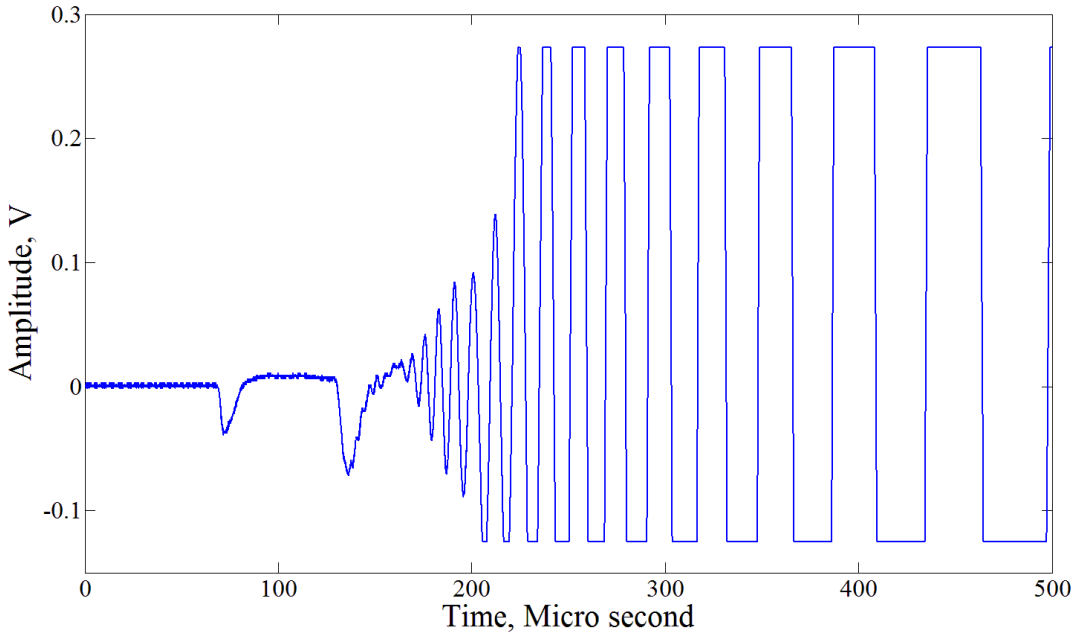

(a)

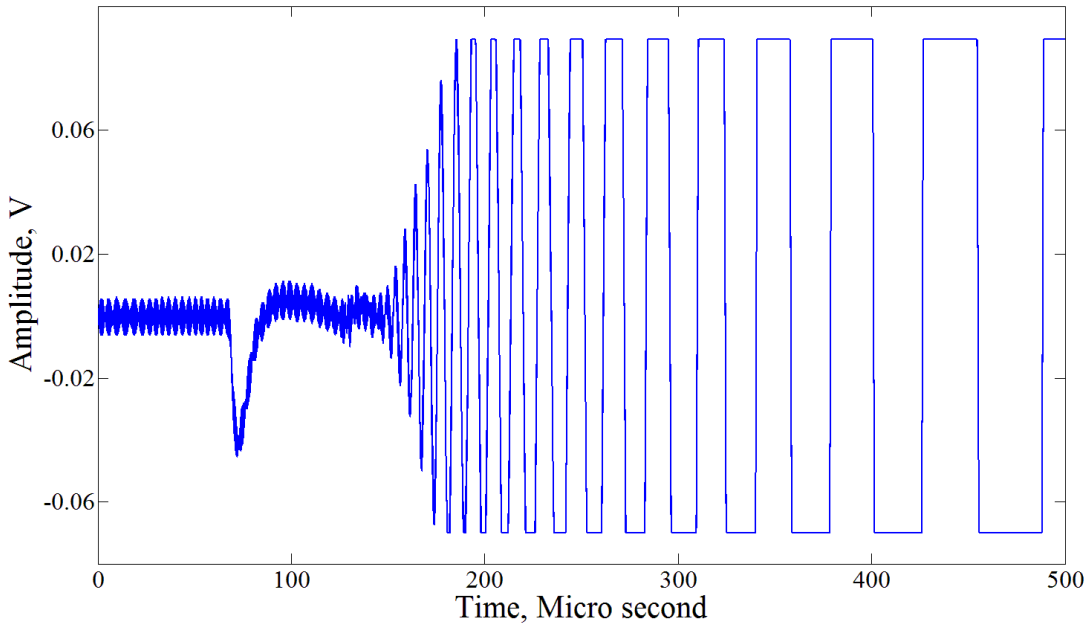

(b)

Figure 4.8. Waveforms captured by sensors for a 45 degree impact at (a) 45 degrees and (b) 0 degrees

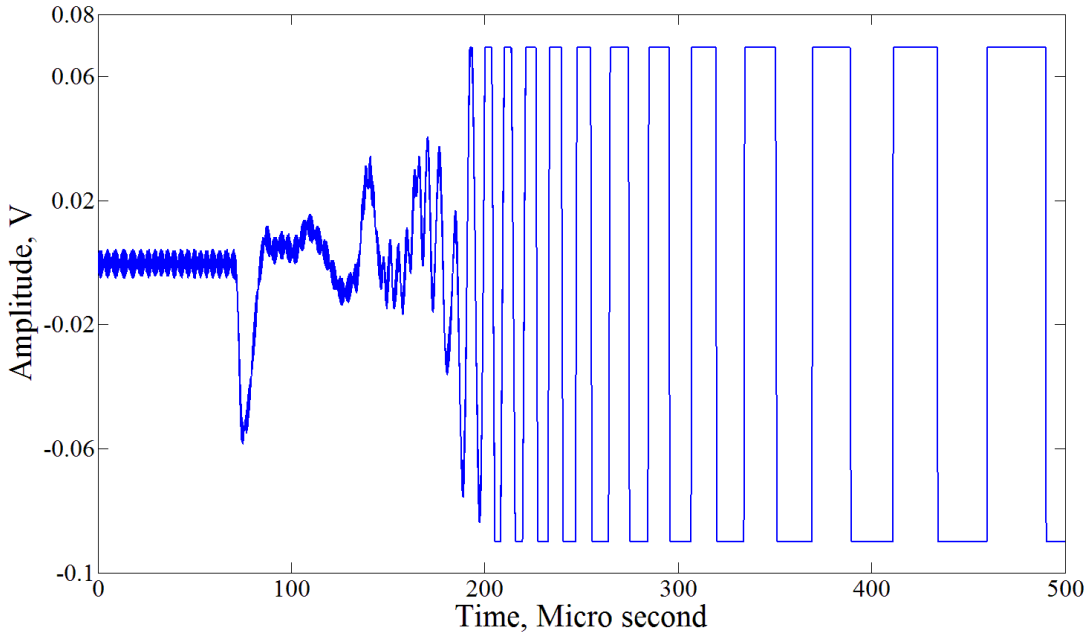

(a)

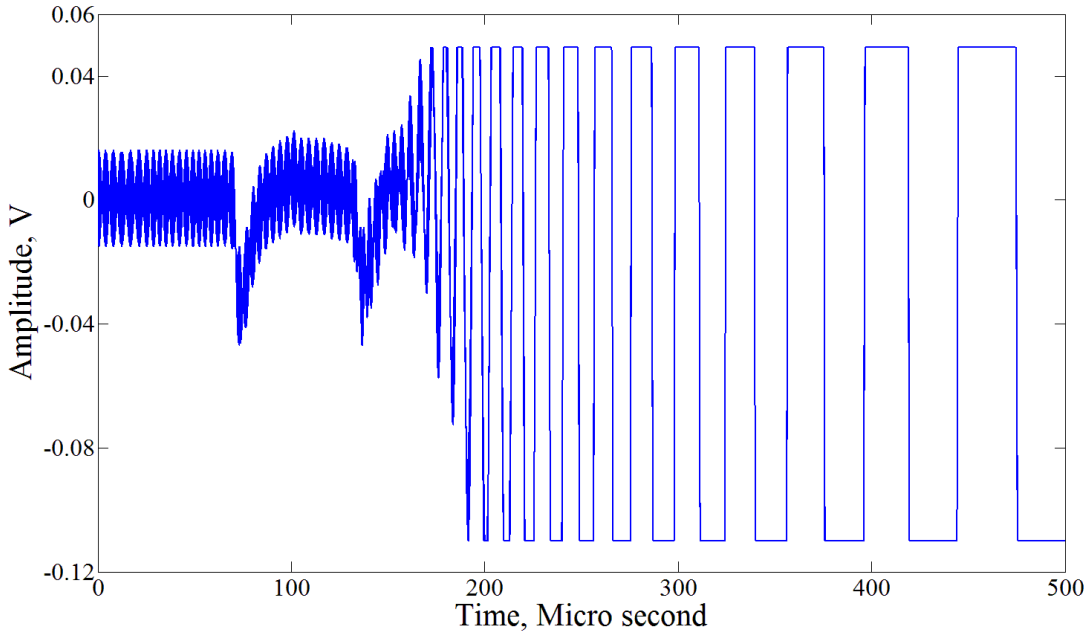

(b)

Figure 4.9. Waveforms captured by sensors for a 45 degree impact at (a) 45 degrees wafer sensor and (b) 30 degrees

Upon closer inspection of the plate after the impact, it was found that the impacts leave a permanent indentation. With the help of a microscope equipped with a camera, the indentations were measured and found to have a diameter of 0.8 mm. (Figure 4.10)

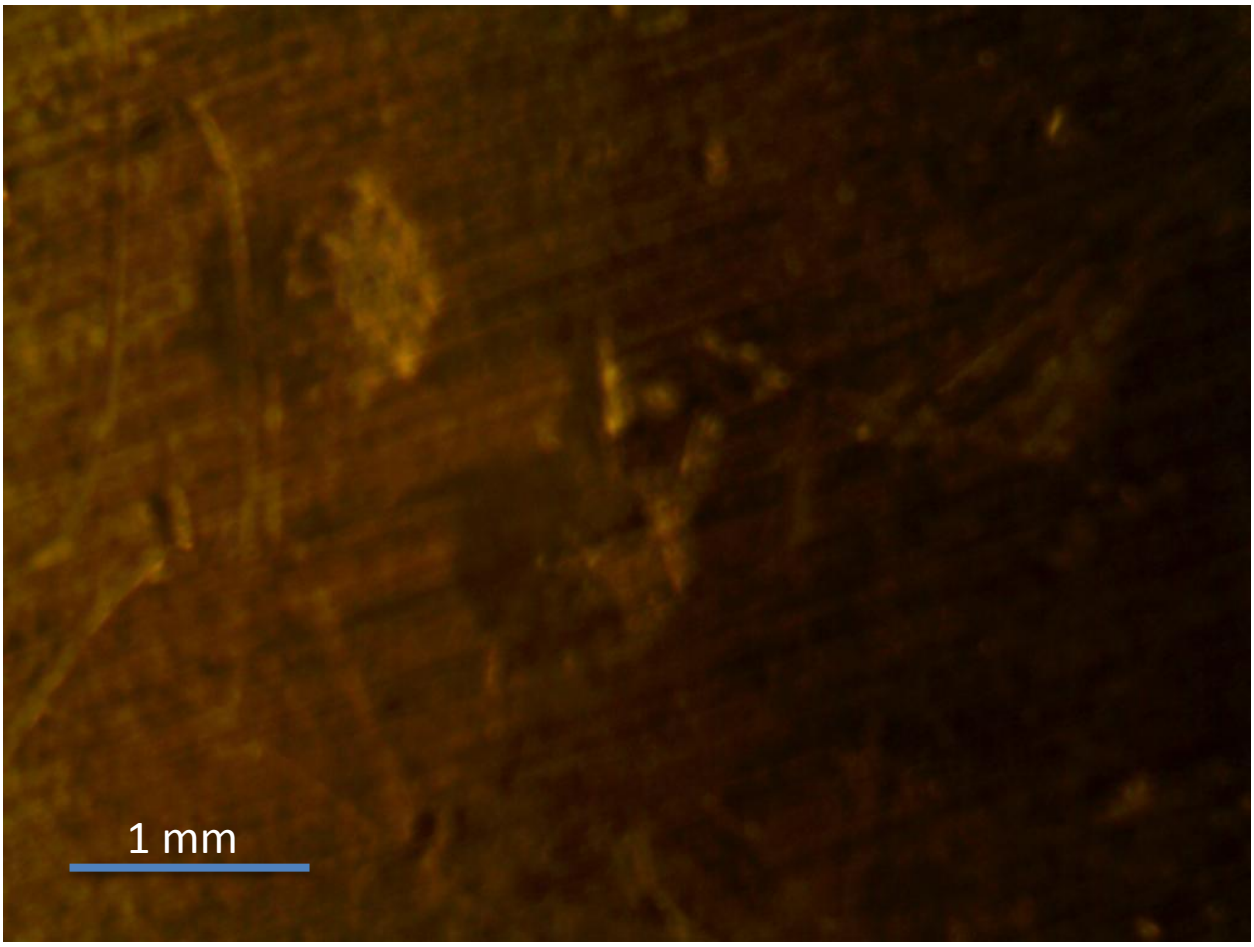

Figure 4.10. Indentations caused by the impacts

From figure 4.10 it can be clearly seen that the impact has created permanent indentations on the Aluminum plate. The plastic deformation during impact was included in the numerical analysis reported in the next chapter.

4.4.1 Experimental observations. Upon analyzing the waveforms that were obtained during the experiment, it was evident that the contact could not be treated as a point contact. This conclusion was derived based on preliminary numerical simulations that were carried out. From

the simulations it was found out that the point loads did not produce the high frequency components of the anti-symmetric mode that was present in the experimental waveforms. The presence of the indentations also indicates the same. In addition to that, it is also evident that the material undergoes plastic transformation.

4.5 High Speed Camera Experiments

In order to estimate the impact duration experimentally, a high speed camera was used to record the impact event. Photron Fastcam with a maximum frame rate of 100,000 fps was used in these experiments. The impact of the ball on the plate was recorded at 50,000 fps (20 μs/frame). Upon analyzing the video frame by frame, it was determined that the impact duration was 60-80 μs (3 to 4 frames). This result agrees with results from the Hertz contact theory. The summary of the results are given in table 4.2.

Table 4.2

Impact Durations Calculated and Observed

Source	Duration/μs
Hertz theory	78
High speed photography	60-80

CHAPTER 5

Numerical Simulation

Finite element technique was used to numerically simulate the impact event in order to understand the physics of the impact and the mechanism of the impact related wave propagation. The commercially available finite element software LS-DYNA was used for this analysis. A sphere of diameter 6 mm, the same as the one used in the experiment was modeled along with an aluminum plate of dimension 1200 mm x 1200 mm x 1.5 mm as in the experiment.

5.1 LS-DYNA

The problem of a steel sphere impacting a square aluminum plate was simulated. The model used the same geometry and material properties that were used in the experiments reported in the last chapter. The diameter of the steel sphere was 6 mm and the dimensions of the aluminum plate were 1200 mm x 1200 mm x 1.5 mm. The plate was clamped along its edges. This software is designed to handle highly nonlinear transient dynamic finite element analysis with many built in material models, element types and contact algorithms. LS-DYNA is widely used in automobile, aerospace, bio engineering, and various other fields. With the aid of the built in material models and contact algorithms many real world problems can be simulated numerically. The latest release, LS-DYNA, version 971, release 6 was used for the numerical simulations.

5.1.1 Contact algorithms. In LS-DYNA, contact is defined by identifying locations that are to be checked for penetration of slave nodes through master surface i.e. slave and master segments have to be defined or would be defined by the contact algorithm itself in order to calculate the contact forces. At each time step of the simulation, the master surface would be checked for penetration by a slave node, and when such penetration is identified, a force

proportional to the penetration will be applied on the slave node in order to resist and ultimately eliminate the penetration. ("Contact medeling in LS-DYNA,")

The resistive forces applied on the nodes are calculated based on the contact stiffness calculated by the contact algorithms. The contact is internally represented by linear springs between the slave nodes and the nearest master segments and the spring stiffness is calculated based on the segment size and the material properties. This method is referred to as the penalty based approach to correctly represent the contact between two surfaces specified by the option SOFT=0.

When dissimilar materials come into contact, the penalty based approach has been found to be inadequate. For these cases, different methods to calculate the spring stiffness have been implemented in LS-DYNA. These methods are called the self-constraint based approach. There are two different algorithms in this self-constraint based approach to calculate the spring stiffness. The first approach divides the nodal masses that come into contact by the square of the time step and using a factor for stability specified by the SOFT=1 option. The stiffness calculated by this method is independent of the material constants and recommended for dissimilar materials whose material properties differ by a large amount. The second approach also uses the mass and time step based stiffness, but applies the loads as the pair of 4 node segments corresponding to the sphere and plate come into contact, and the loads are applied to all 8 nodes (SOFT=2).

While the above mentioned methods are used to calculate the contact forces, there are different ways in which contact is defined in LS-DYNA. The term ‘automatic’ that occurs in the contact title stands to define that the penetrations that come from any direction will be identified

by the algorithm itself. Some of the most widely used and suitable contact types for this problem are given below.

- CONTACT_AUTOMATIC_NODES_TO_SURFACE
- CONTACT_AUTOMATIC_SURFACE_TO_SURFACE
- CONTACT_AUTOMATIC__SINGLE_SURFACE

CONTACT_AUTOMATIC_NODES_TO_SURFACE is defined as a one way treatment of contact. I.e. the nodes from the slave part would be checked for penetration through the master surface. In the CONTACT_AUTOMATIC_SURFACE_TO_SURFACE at each time step both contacting parts would take the role of master and slave and forces would be calculated and applied on the nodes of each part. CONTACT_AUTOMATIC__SINGLE_SURFACE is an even more advanced option where all the contacting parts are considered as slave parts together and all the surfaces would be checked for penetration including self-contact. The SOFT=2 option is only available for the SURFACE_TO_SURFACE contact options. But it is expected to give a more realistic force distribution.

5.1.2 Material models. There are numerous material models available in LS-DYNA in order to accommodate different materials and various real world scenarios. The available models cover the instances of purely elastic deformations, deformations that go into the plastic region, orthotropic materials, materials with visco-elastic properties etc. and these materials are further developed with options for failure, thermal simulations etc. Due to the observed plastic deformations during the experiment, it was decided to use the MATERIAL_PIECEWISE_LINEAR_PLASTIC for the plate in the numerical simulations. The properties assigned to the material are listed in table 5.1.

Table 5.1

Material Properties

Part	Material	Material type	Density, kg/m^3	Poisson's ratio	Young's modulus,GPa	Yield strength
Plate	Aluminum	Linear plastic	2.7	0.3	75	0.2 %
Sphere	Steel	Elastic	7.65	0.3	207	

5.1.3 Hourglass control. In LS-DYNA, under-integrated elements go through non-physical modes of deformation during numerical simulations. It becomes necessary to eliminate those modes, which are known as hourglass modes, in order to obtain accurate results. LS-DYNA provides different types of hourglass controlling methods and coefficients to inhibit the hourglass modes. These controlling algorithms calculate the deformation and apply a counter acting force to eliminate these modes. For solid elements, it is recommended that the hourglass formulation 6 be used with an hourglass coefficient of 1. ("LS-DYNA Aerospace working group Modeling guidelines," 2012)

5.2 Modeling

An aluminum plate of dimensions 1200 mm x 1200 mm x 1.5 mm was modeled with eight node brick elements that have one integration point. As explained earlier, in order to overcome the complex hourglass effects an hourglass formulation 6 with an hourglass coefficient 1 was activated in the model.

Upon analyzing the results from the preliminary simulations, it was evident that the element size influences the results. Larger elements (0.5 mm x 0.5 mm) gave rise to multiple S_0 and A_0 components when each of the nodes of the plate comes into contact with the impacting object. Figure 5.1 demonstrates the results of multiple impacts in the simulation.

It was concluded that in order to simulate a realistic load distribution, the elements in the contact region needs to be as small as possible. The amount of achievable refinement was limited by the available computing power. Therefore, the contact region was meshed with elements of dimension 0.0625 mm x 0.0625 mm and the rest of the plate was modeled with graded mesh with a ratio of 0.96.

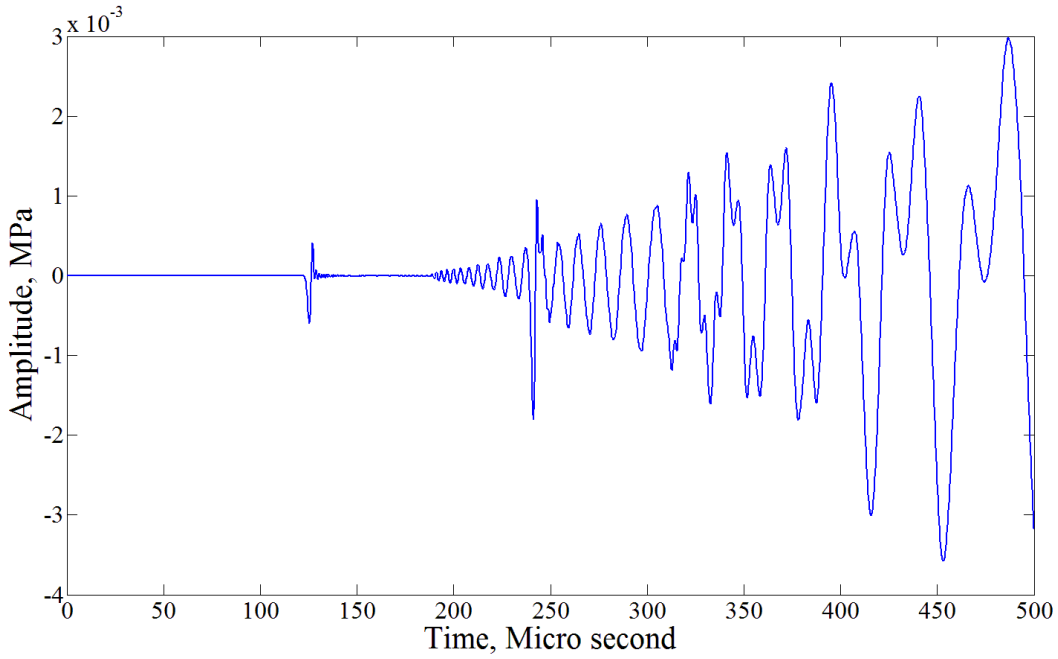

Figure 5.1. Waveform for a 0 degree impact from the simulation

5.2.1 Model. The plate model used in the simulation is shown in figure 5.2. Impact was restricted to the area with the fine mesh. In figure 5.3 the end view of the plate and ball is shown. The sphere was modeled with matching element size and placed 1 mm above the top surface of the plate and the impact velocity was assigned as the initial condition. The termination time was assigned as 500 μs. The controls and parameters that affect the results are identified as: contact definition, friction, and mesh size. A summary of the controls used for various simulations are given in table 5.2.

Table 5.2

Summary of Simulations

Model	Contact	SOFT	Friction	Hourglass	Figure
1	NTS	0	No	Yes	5.4
2	NTS	0	Yes	Yes	
3	NTS	1	No	Yes	
4	NTS	1	Yes	Yes	
5	STS	0	No	Yes	
6	STS	0	Yes	Yes	
7	STS	1	No	Yes	5.5(a)
8	STS	1	Yes	Yes	5.5(b)
9	STS	2	No	Yes	5.6(a)
10	STS	2	Yes	Yes	5.6(b)

NTS – CONTACT_AUTOMATIC_NODES_TO_SURFACE

STS – CONTACT_AUTOMATIC_SURFACE_SURFACE

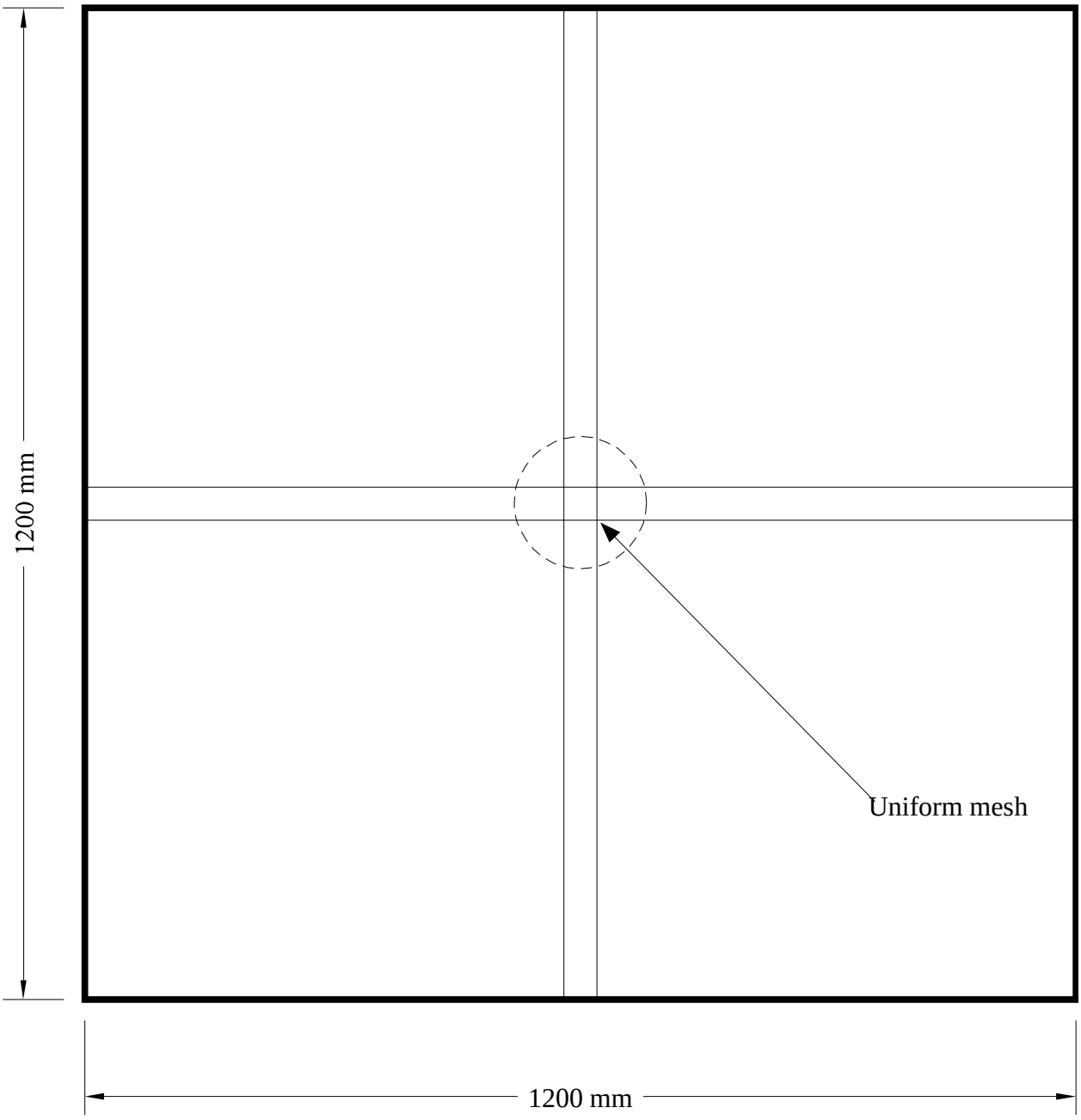

Figure 5.2. Model used for the numerical simulation

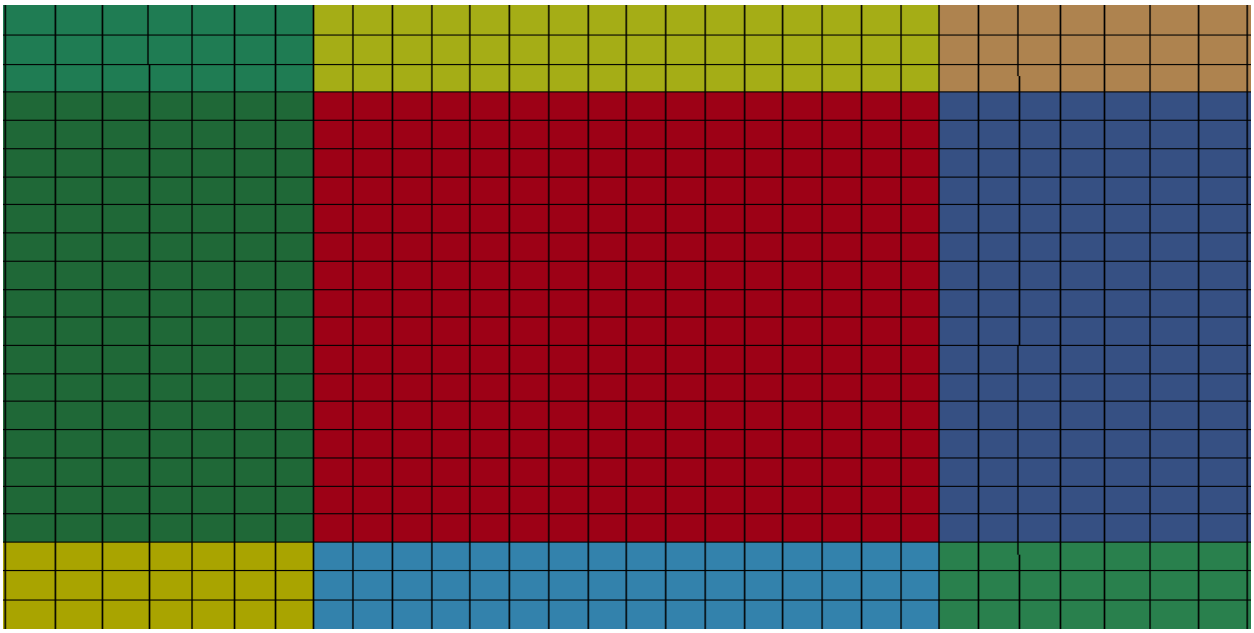

(a)

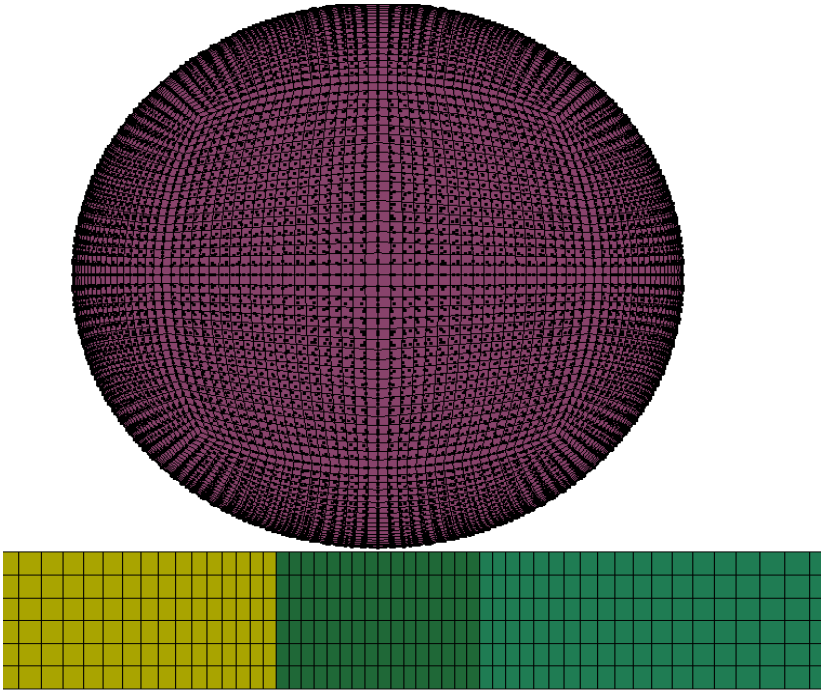

(b)

Figure 5.3. Model used for the numerical simulation (a) Closeup on the fine mesh (b) Side view of the sphere

5.2.2 Results from the simulations. The results obtained from the simulations, by changing the various parameters that control the simulation are given below. Figure 5.4 shows the waveform extracted from the simulation with CONTACT_AUTOMATIC-NODES_TO_SURFACE option, no hourglass control, and piecewise smooth linear plastic material with 0.2% yield stress. Further, no friction coefficients were assigned.

The parameters used to compare the waveforms from the simulations and the experiments are: The amplitude ratio S_0/A_0 and the frequency content of the components. A higher S_0/A_0 ratio implies higher ratio of in-plane load/normal load.

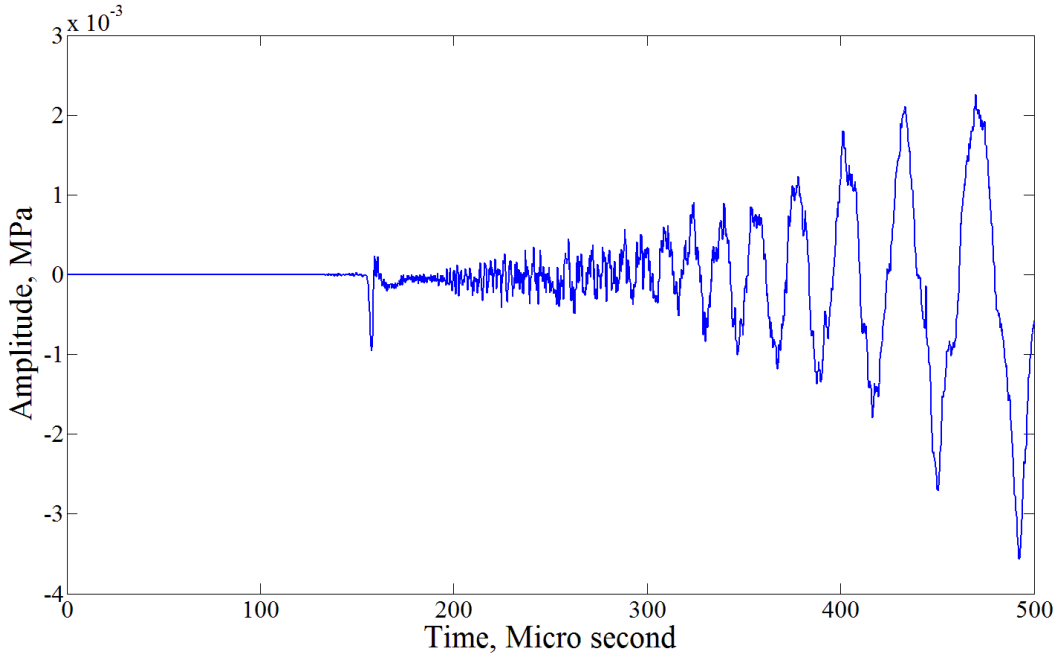

Figure 5.4. Waveform for a 0 degree impact from the simulation

Upon analyzing the waveforms shown in figures 5.4 and 5.5, the amplitude ratio S_0/A_0 was found to be 0.3, which is 50 times higher than what was obtained in the experiments. From this it was concluded that the contact algorithms and the other control parameters used in models 1, 7 and 8 introduced larger in-plane loads than what was present in the experiment. The contact durations estimated from models 1, 7 and 8 were in the order of 400 μs.

Results from models 7 and 8 (Figure 5.6) provided an amplitude ratio of 0.069, which is 10 times higher than the ones from the experiment, also it was found that the contact duration is relatively large (300 µs) compared to that of the experiment (80 µs).

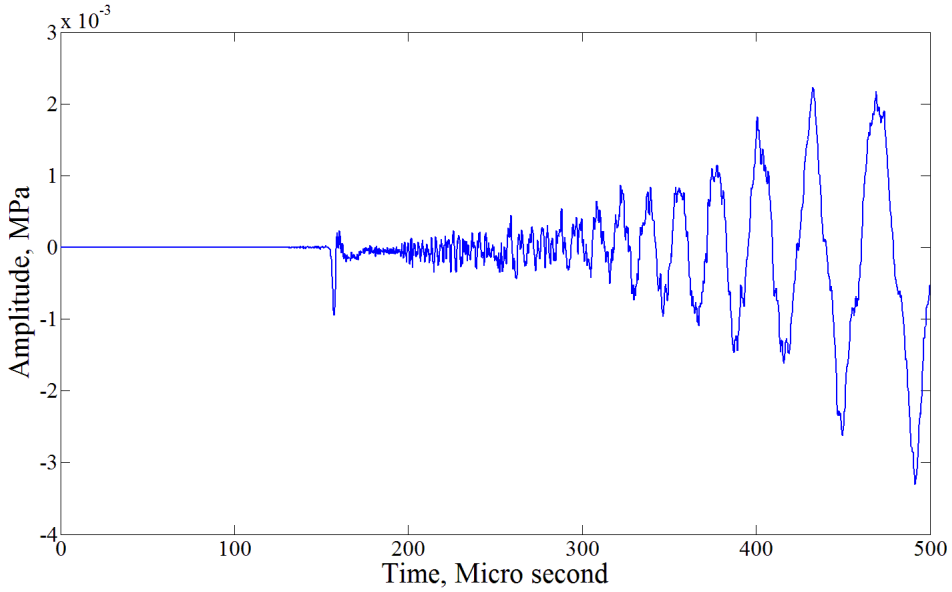

(a)

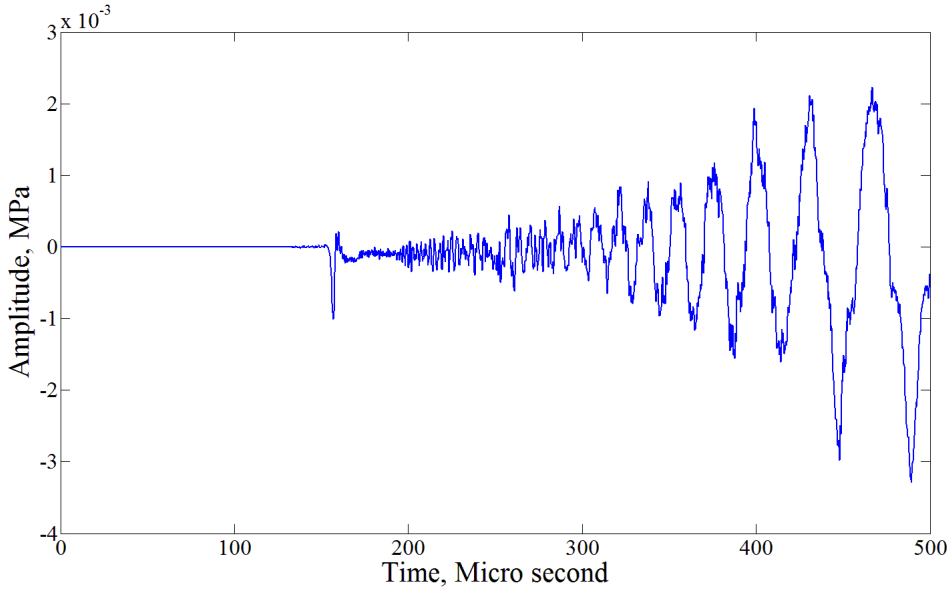

(b)

Figure 5.5. Waveform for a 0 degree impact from the simulation (a) Model 7 (b) Model 8

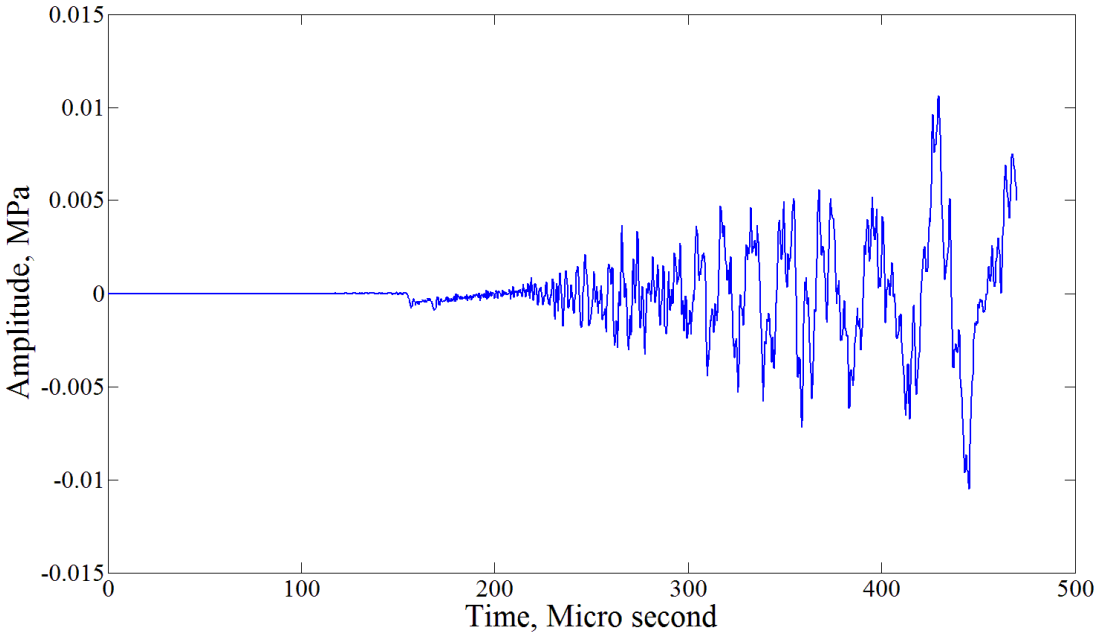

(a)

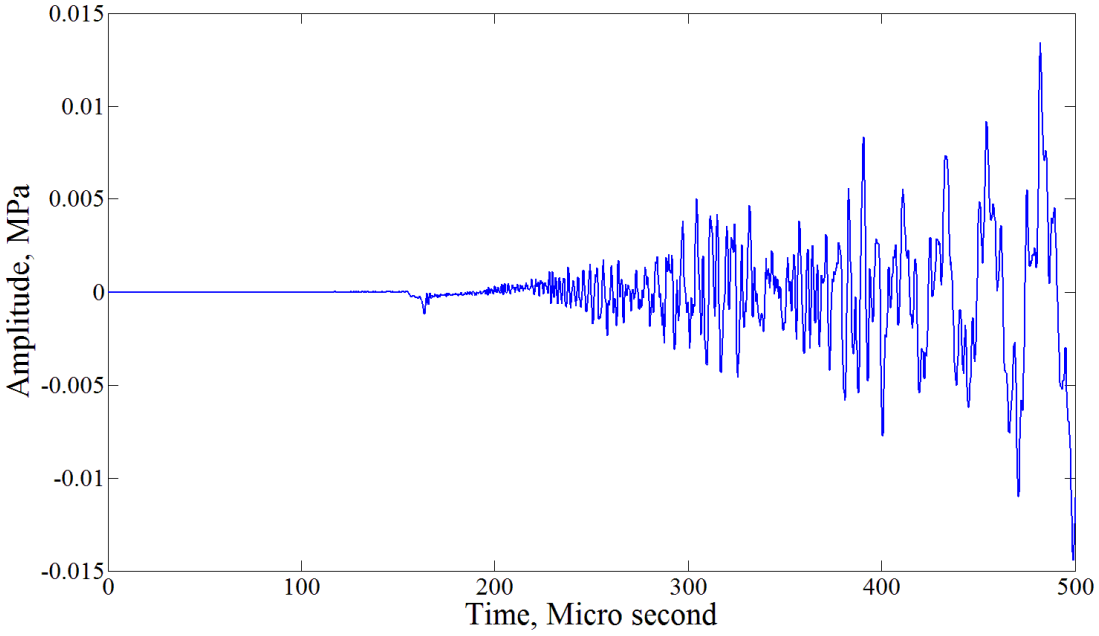

(b)

Figure 5.6. Waveform for a 0 degree impact from the simulation (a) Model 9 (b) Model 10

5.2.3 Summary of results. The important observations from the impact simulations are listed below.

- Contact algorithms used in the simulation with SOFT=0 and SOFT=1 options produce larger in-plane loads compared to that of the experiment
- CONTACT_AUTOMATIC_SURFACE_TO_SURFCE algorithm with SOFT=2 option provides more realistic load distribution, but shows longer contact duration. Hence produces different frequency content

From these simulations, it was evident that the contact algorithms in the LS-DYNA program are inadequate to represent the actual impact as far as the wave propagation is concerned. Therefore further simulations were carried out based on the Hertz's contact theory. The equations were used to calculate the duration and the pressure distribution during the impact and the loads were distributed at the nodes of the axisymmetric model of the plate.

CHAPTER 6

Axisymmetric Simulation

During the impact between a plate and a sphere, the contact surfaces deform and form a curved surface. In this particular case of steel and aluminum, the deformation of the steel can be neglected. The solution to the static contact problem was adapted to the dynamic impact problem by Abrate (Abrate, 2001). With this solution, the impact problem can be simplified to one where a dynamic load is being applied to the sphere. The applied load, F is calculated based on the material properties and initial conditions. Due to the curvature of the contact surface, the loads transferred to the plate have in-plane components. This is illustrated in figure 6.1.

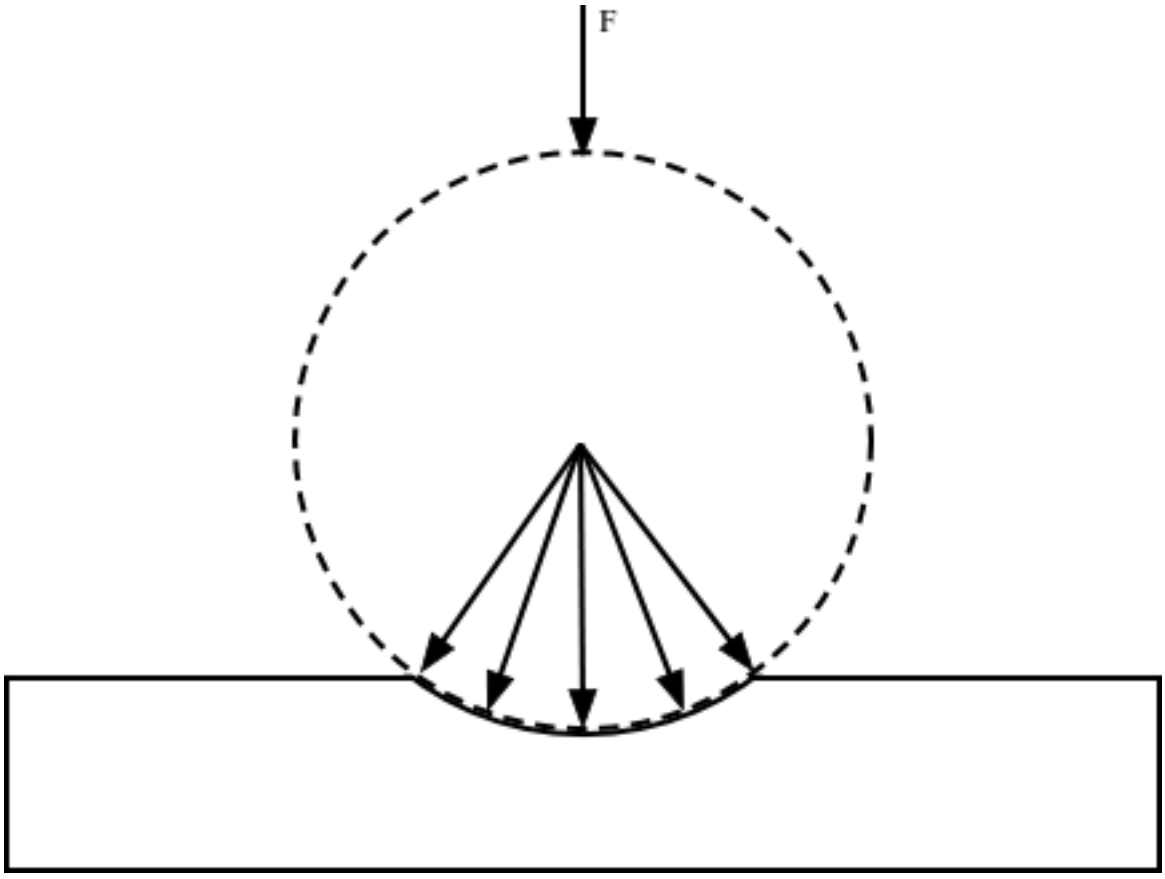

Figure 6.1. Load distribution on the plate during impact

The impact load, F calculated based on the Abrate's solution is shown in figure 6.2. Once F was calculated, the pressure distribution in the contact region is determined. An axisymmetric model of the plate was generated using PreSys, a commercially available modeling software, with the dimensions 1.5 mm x 800 mm with 0.25 mm x 0.25 mm elements and the same material properties as of the 3D ball impact simulation were assigned. LS-DYNA element formulation 14 (Area weighted axisymmetric solid) was used with Y axis as the axis of rotation. The nodal loads were determined based on the calculated pressure distribution and the curvature of the contact surface.

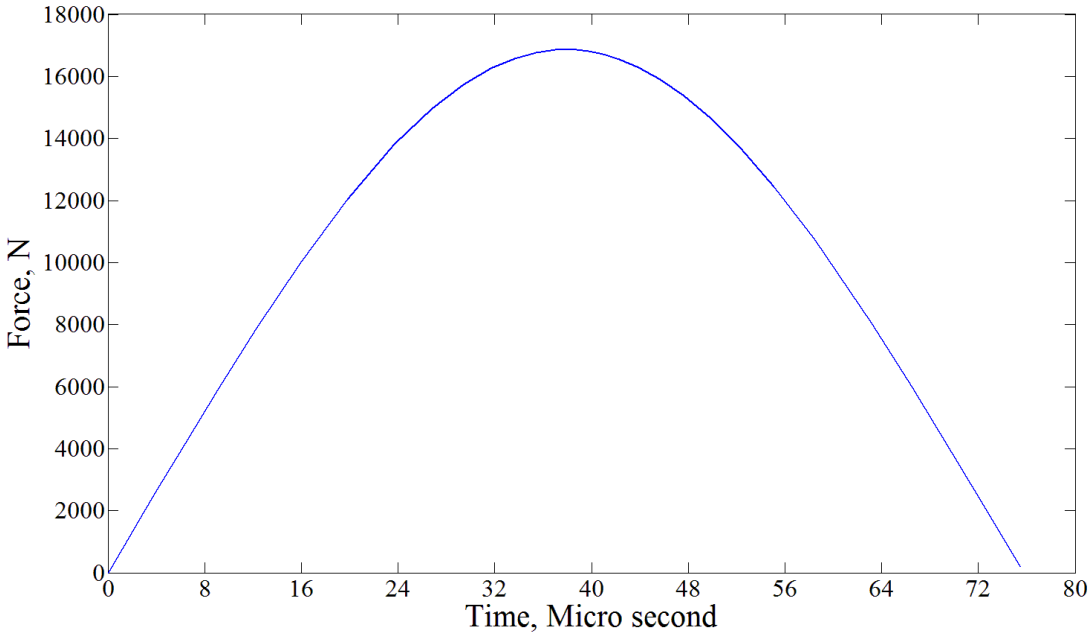

Figure 6.2. Impact load calculated according to Hertz contact theory

In order to simulate the actual load distribution, the inclined loads in the contact region were resolved into in-plane and normal components and applied on the nodes. The load distribution as applied in the numerical simulation is shown in figure 6.3. Loads were applied on the nodes that were in the contact region. The termination time was set as 500 μs, the same duration as the signals recorded during the experiment.

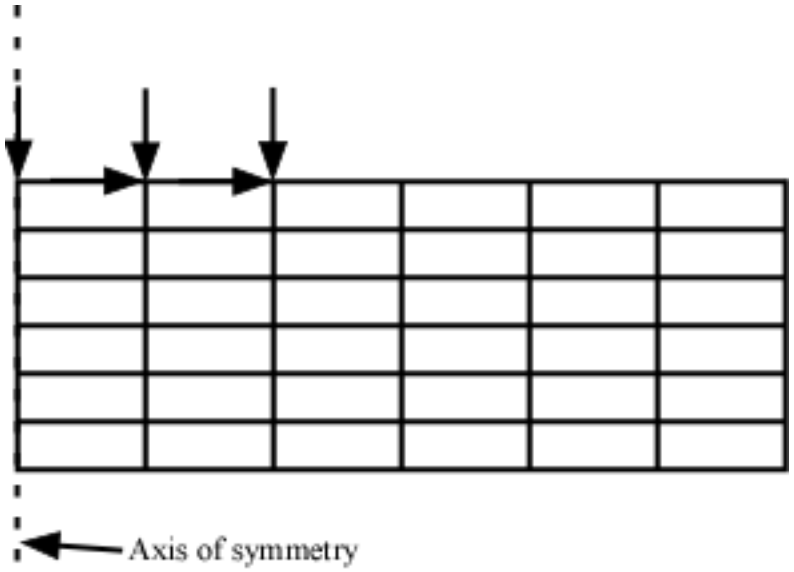

Figure 6.3. Load distribution in the numerical model

The waveform recorded at 450 mm from the point of impact is shown in figure 6.4. In order to demonstrate the accuracy of the results S_0 components from both experiment and the numerical simulation are compared in figure 6.5

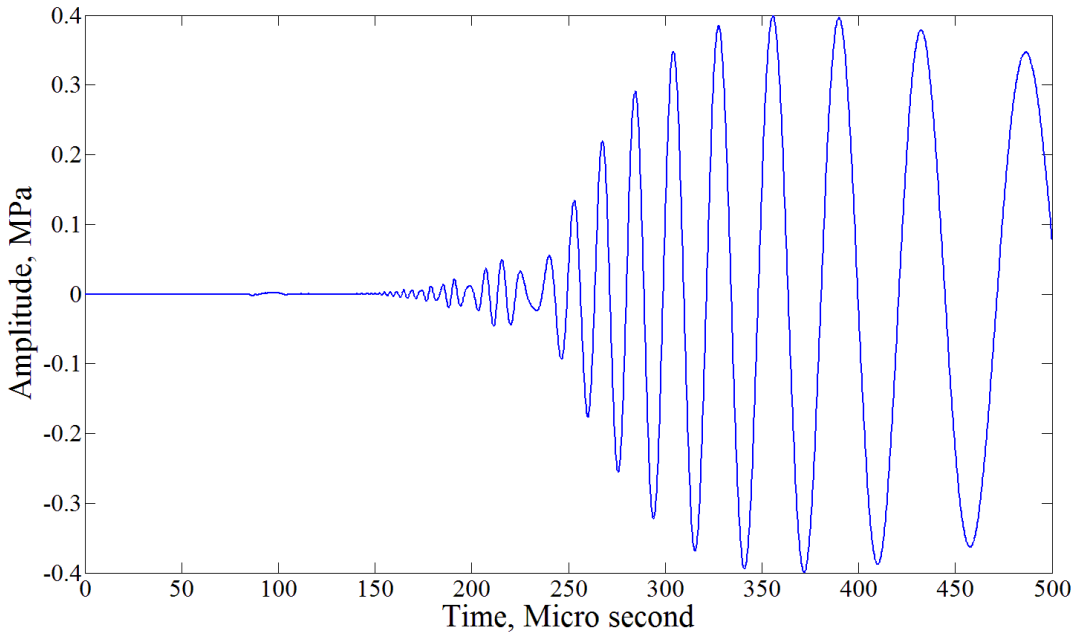

Figure 6.4. Waveform obtained from the axisymmetric model

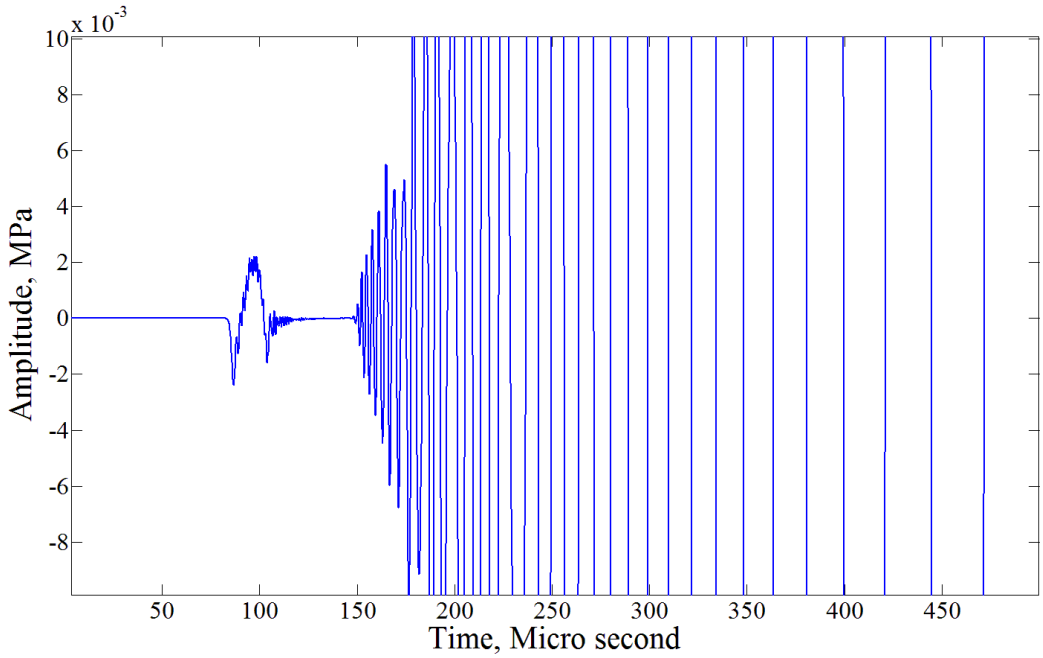

(a)

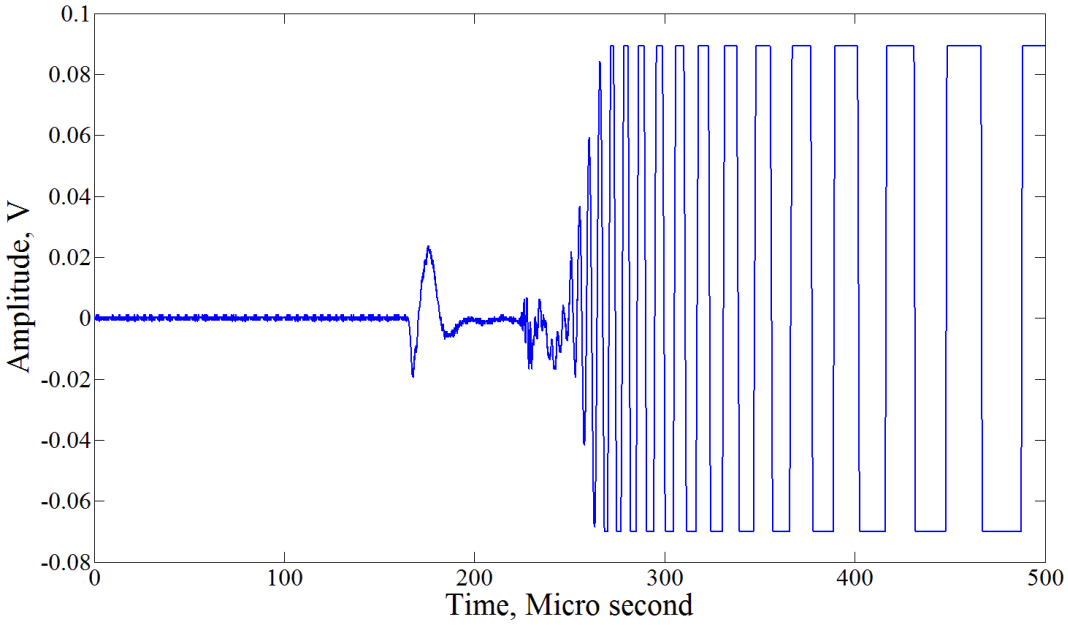

(b)

Figure 6.5. Comparison of numerical and experimental waveforms for normal impact (a) Numerical simulation (b) Experiment

From figure 6.5 it is obvious that the waveforms obtained through the axisymmetric model displays close similarity to the experimental waveforms and the amplitude ratio of the symmetric mode and anti-symmetric mode was found to be 0.005 which is of the same order as the one calculated in the experiment. The frequency content of the waveforms was analyzed using the wavelet transformation.

By looking at the transformations (Figures 6.6 and 6.7), it is obvious that the experimental and the simulated waveforms contain similar frequency content and amplitude ratios. The higher frequencies that appear later in the experimental waveform could be attributed to the reflections from the edges.

From these results it is obvious that modeling the normal impact by applying the distributed loads, as opposed to contact modeling in LS-DYNA, provides more accurate S_0 and the high frequency A_0 components. The same method can be extended to oblique impacts by including Maw's solution (Maw et al., 1976) in calculating the impact loads. An axisymmetric model becomes impossible in the case of an oblique impact and a suitable mesh needs to be chosen in order to represent the circular impact region.

Even though the leading edge of the impact signal consists of low amplitude components, they become important in the actual applications of AE based SHM. Due to the noise induced by the vibration of the structures, use of frequencies below 50 kHz is not practical in field applications. Further, these low frequency components are not expected to give important features of the impact, as in the case of an irregularly shaped object where the high frequency leading edge consist of features indicating multiple impacts . Therefore, it becomes necessary to rely on the high frequency components of the signal. Hence, the results obtained from the axisymmetric simulation are more accurate and serves the practical purpose of SHM.

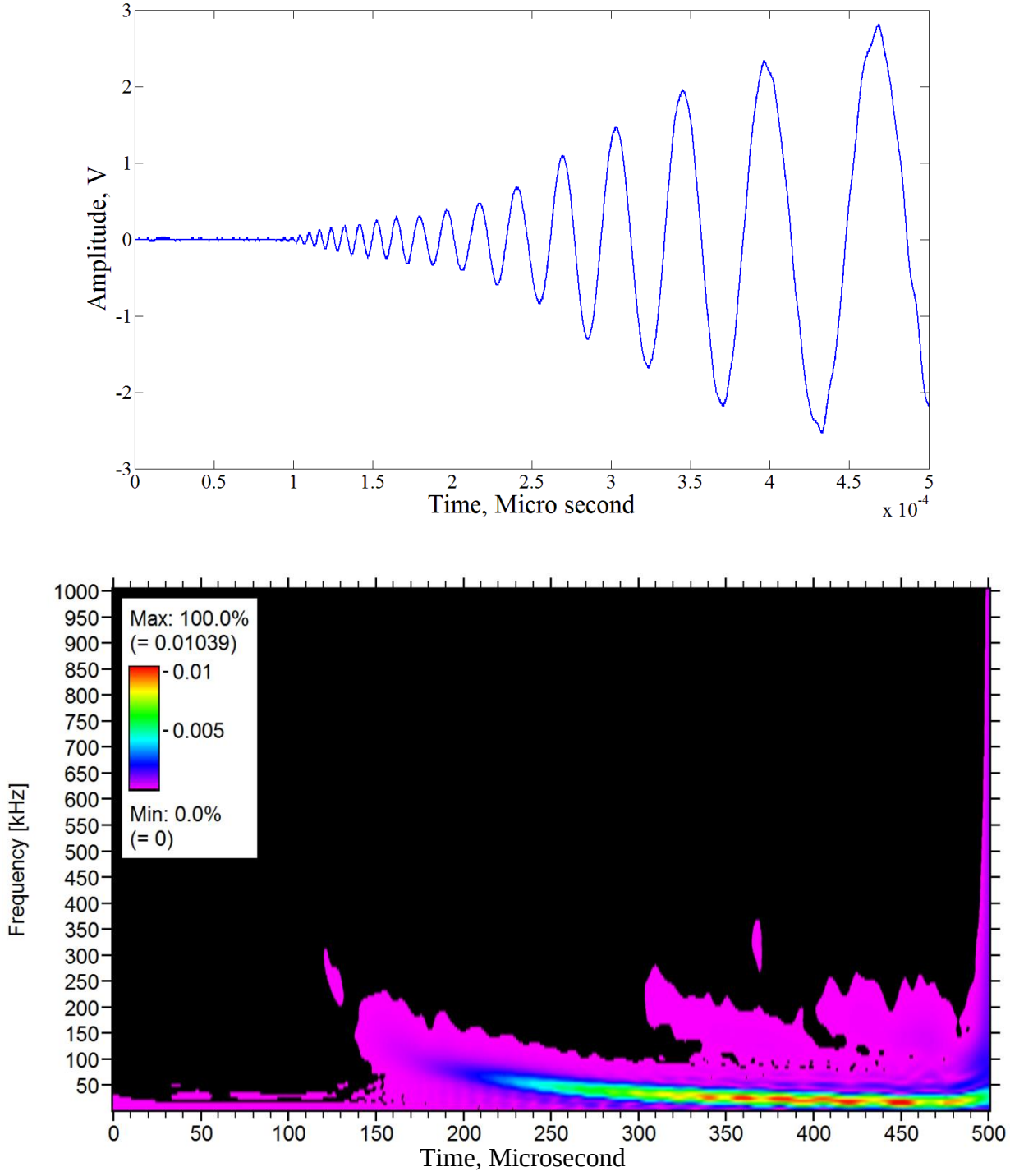

Figure 6.6. Waveform obtained from the experiment and the wavelet (Normal Impact)

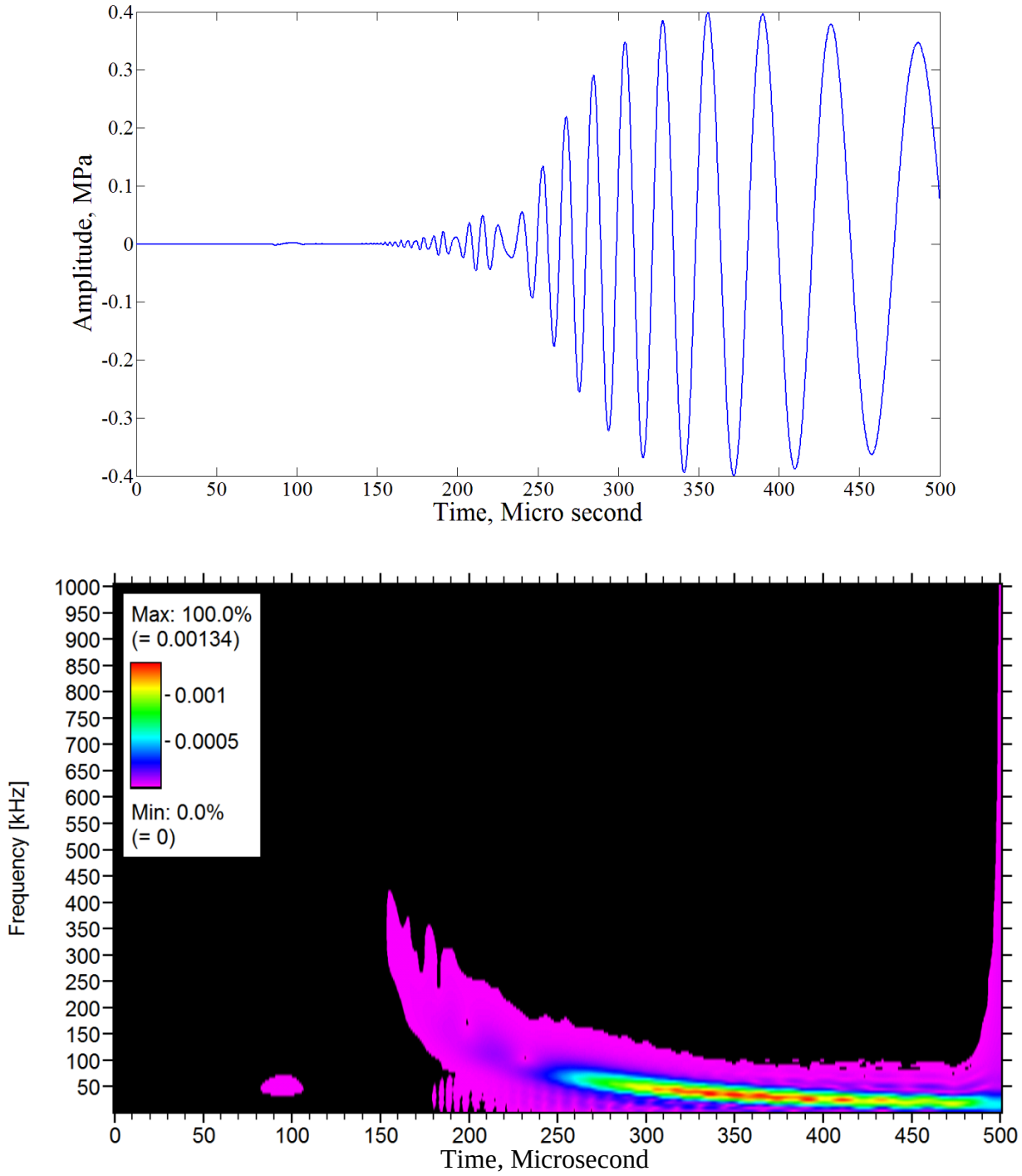

Figure 6.7. Waveform obtained from the axisymmetric model and the wavelet (Normal impact)

CHAPTER 7

Discussion and Future Research

In this research it is shown that the Hertz contact theory provides a better representation of the impact force history for low velocity, non-damage causing impacts. This has been verified by comparing the waveforms collected during experiments and numerical simulations. Further it also has been verified that the impact should not be treated as a point contact. This becomes critical in the case of large object impacts. The presence of the shear horizontal component of the lamb waves has also been verified through the experimental results. By analyzing impacts of varying angles, it is possible to identify the angle of the impact with the aid of the shear horizontal waves.

This research could be extended to incorporate the calculation of impact force history for an inclined impact, which has not been addressed by many. This research was confined to impacts on aluminum panels. With the increasing use of composite panels in aircraft structures, it becomes necessary to extend this study into composite structures. Due to the non-homogeneity of the material, and high level of attenuation, the impact problem becomes even more complicated. A number of studies suggest that Hertz contact theory could be used to calculate impact load history in composite structures. It will be a challenging task to relate the impact mechanism to the stress waves produced in composite materials.

References

Abrate, Serge. (1998). *Impact on Composite Structures* (First ed.). New York: Cambridge University Press.

Abrate, Serge. (2001). Modeling of impacts on composite structures. *Composite Structures, 51*(2), 129-138. doi: 10.1016/s0263-8223(00)00138-0

Bartoli, I., Salamone, S., Di Scalea, F.L., Rhymer, J., & Kim, H. (2011). *Impact force identification in aerospace panels by an inverse ultrasonic guided wave problem.* Paper presented at the Society of Photo-Optical Instrumentation Engineers (SPIE) Conference Series.

Batra, R. C., Gopinath, G., & Zheng, J. Q. (2012). Damage and failure in low energy impact of fiber-reinforced polymeric composite laminates. *Composite Structures, 94*(2), 540-547. doi: 10.1016/j.compstruct.2011.08.015

Baxter, Matthew Geoffrey, Pullin, Rhys, Holford, Karen M., & Evans, Sam L. (2007). Delta T source location for acoustic emission. *Mechanical Systems and Signal Processing, 21*(3), 1512-1520. doi: 10.1016/j.ymssp.2006.05.003

Boyce, B. L., Chen, X., Hutchinson, J. W., & Ritchie, R. O. (2001). The residual stress state due to a spherical hard-body impact. *Mechanics of Materials, 33*(8), 441-454. doi: 10.1016/s0167-6636(01)00064-3

Chunlin, Chen, & Fuh-Gwo, Yuan. (2010). Impact source identification in finite isotropic plates using a time-reversal method: theoretical study. *Smart Materials and Structures, 19*(10), 105028.

Ciampa, F., & Meo, M. (2010). Acoustic emission source localization and velocity determination of the fundamental mode A 0 using wavelet analysis and a Newton-based optimization technique. *Smart Materials and Structures, 19*(4), 045027.

Contact medeling in LS-DYNA.). Retrieved October 11, 2013, from http://www.dynasupport.com/tutorial/contact-modeling-in-ls-dyna

Hajzargerbashi, Talieh, Kundu, Tribikram, & Bland, Scott. (2011). An improved algorithm for detecting point of impact in anisotropic inhomogeneous plates. *Ultrasonics, 51*(3), 317-324. doi: 10.1016/j.ultras.2010.10.005

Howard, M. Matt, & Francesco Lanza di, Scalea. (2007). Macro-fiber composite piezoelectric rosettes for acoustic source location in complex structures. *Smart Materials and Structures, 16*(4), 1489.

Hu, N., Fukunaga, H., Matsumoto, S., Yan, B., & Peng, X. H. (2007). An efficient approach for identifying impact force using embedded piezoelectric sensors. *International Journal of Impact Engineering, 34*(7), 1258-1271. doi: 10.1016/j.ijimpeng.2006.05.004

Hyunjo, Jeong, & Young-Su, Jang. (2000). Fracture source location in thin plates using the wavelet transform of dispersive waves. *Ultrasonics, Ferroelectrics and Frequency Control, IEEE Transactions on, 47*(3), 612-619. doi: 10.1109/58.842048

Inoue, H., Harrigan, J.J., & Reid, S.R. (2001). Review of inverse analysis for indirect measurement of impact force. *Applied Mechanics Reviews, 54*, 503.

Johnson, K.L. (1985). *Contact Mechanics* (First ed.). Cambridge: Cambridge University Press.

LS-DYNA Aerospace working group Modeling guidelines. (2012, June 1,2012). from http://awg.lstc.com/tiki/tiki-index.php

Maw, N., Barber, J. R., & Fawcett, J. N. (1976). The oblique impact of elastic spheres. *Wear, 38*(1), 101-114. doi: http://dx.doi.org/10.1016/0043-1648(76)90201-5

Menna, Costantino, Asprone, Domenico, Caprino, Giancarlo, Lopresto, Valentina, & Prota, Andrea. (2011). Numerical simulation of impact tests on GFRP composite laminates. *International Journal of Impact Engineering, 38*(8–9), 677-685. doi: 10.1016/j.ijimpeng.2011.03.003

Mindlin, R. D., & Deresiewicz, H. (1953). ELASTIC SPHERES IN CONTACT UNDER VARYING OBLIQUE FORCES. *Journal of Applied Mechanics-Transactions of the Asme, 20*(3), 327-344.

Park, Byeongjin, Sohn, Hoon, Olson, Steven E, DeSimio, Martin P, Brown, Kevin S, & Derriso, Mark M. (2012). Impact localization in complex structures using laser-based time reversal. *Structural Health Monitoring, 11*(5), 577-588. doi: 10.1177/1475921712449508

Roy, Surajit, Mueller, Ingolf, Janapati, Vishnuvardhan, Das, Samik, & Chang, Fu-Kuo. (2012). Real-time prediction of impact-induced damage for composite structures based on failure analysis and efficient database methods. 83481L-83481L. doi: 10.1117/12.917528

Setoodeh, A. R., Malekzadeh, P., & Nikbin, K. (2009). Low velocity impact analysis of laminated composite plates using a 3D elasticity based layerwise FEM. *Materials & Design, 30*(9), 3795-3801. doi: 10.1016/j.matdes.2009.01.031

Shim, V. P. W., Guo, Y. B., & Tan, V. B. C. (2012). Response of woven and laminated high-strength fabric to oblique impact. *International Journal of Impact Engineering, 48*, 87-97. doi: 10.1016/j.ijimpeng.2011.06.008

Worden, K., & Staszewski, W. J. (2000). Impact Location and Quantification on a Composite Panel using Neural Networks and a Genetic Algorithm. *Strain, 36*(2), 61-68. doi: 10.1111/j.1475-1305.2000.tb01175.x

Appendix

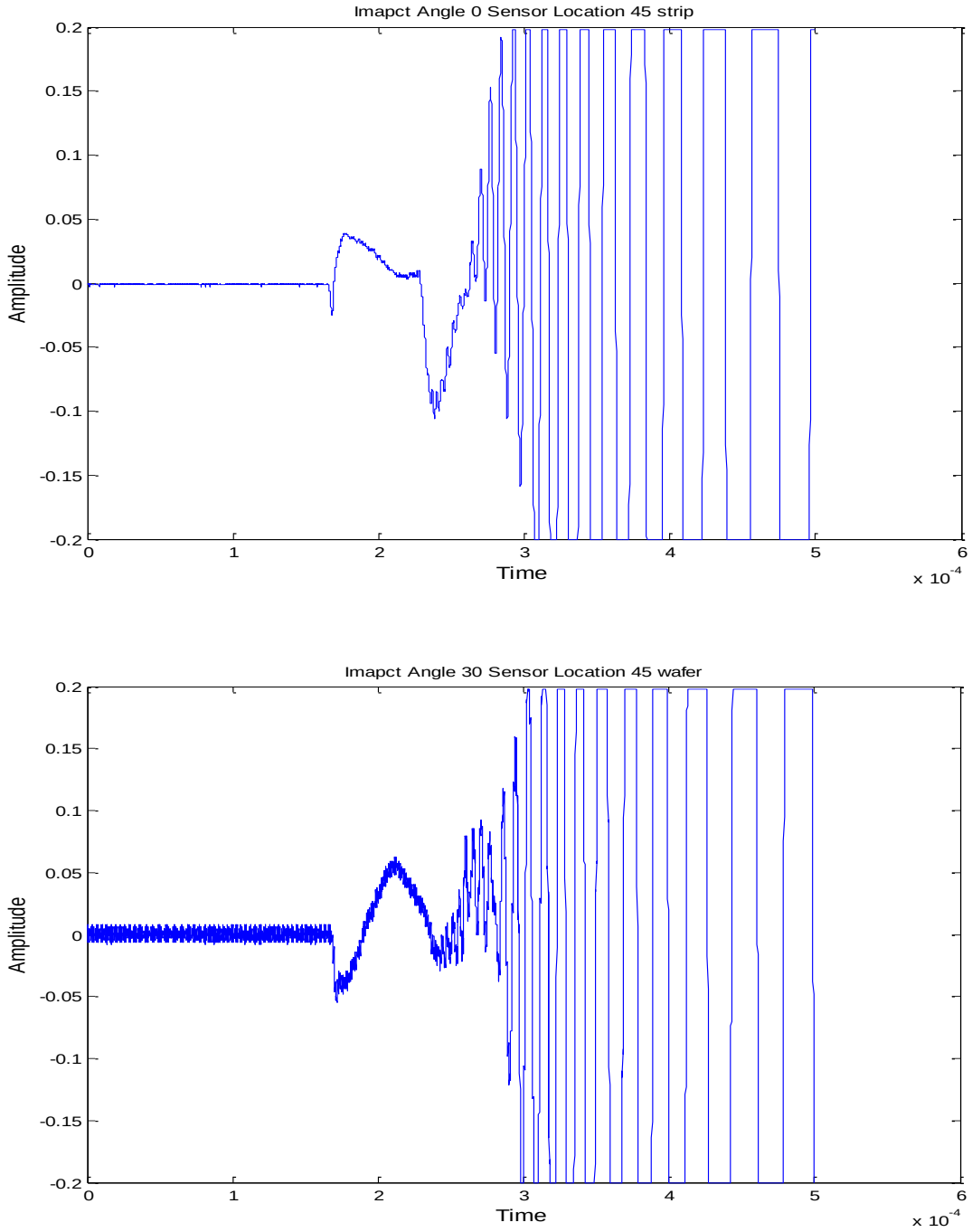

Waveforms captured by the sensors at 45 degrees and 0 degree for a normal impact by a 20 mm diameter ball

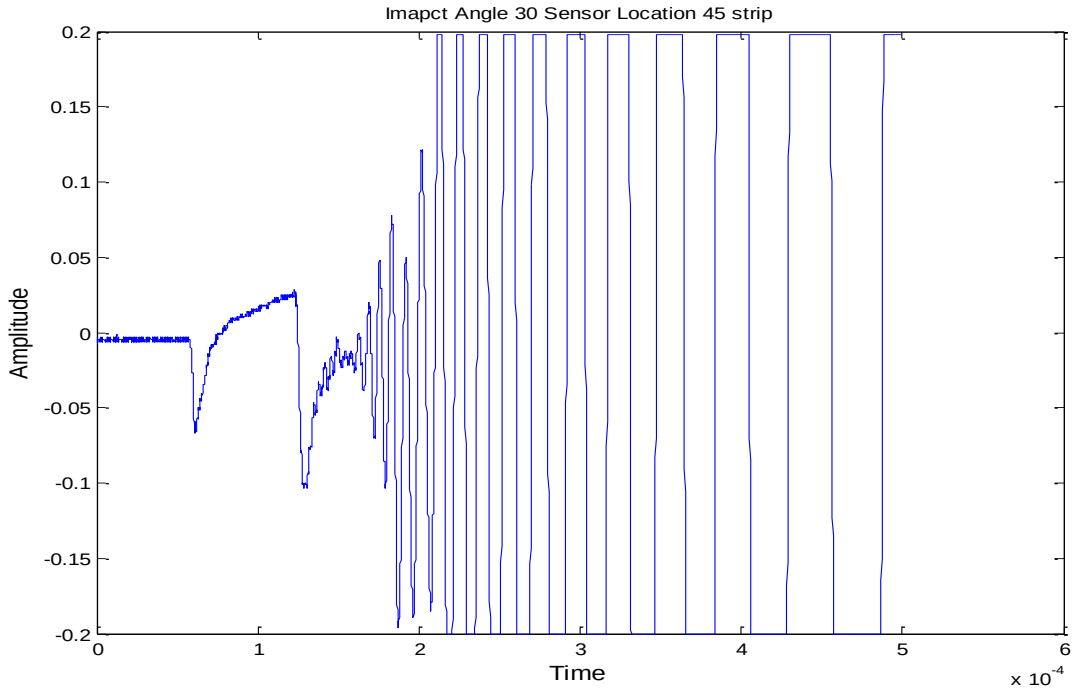

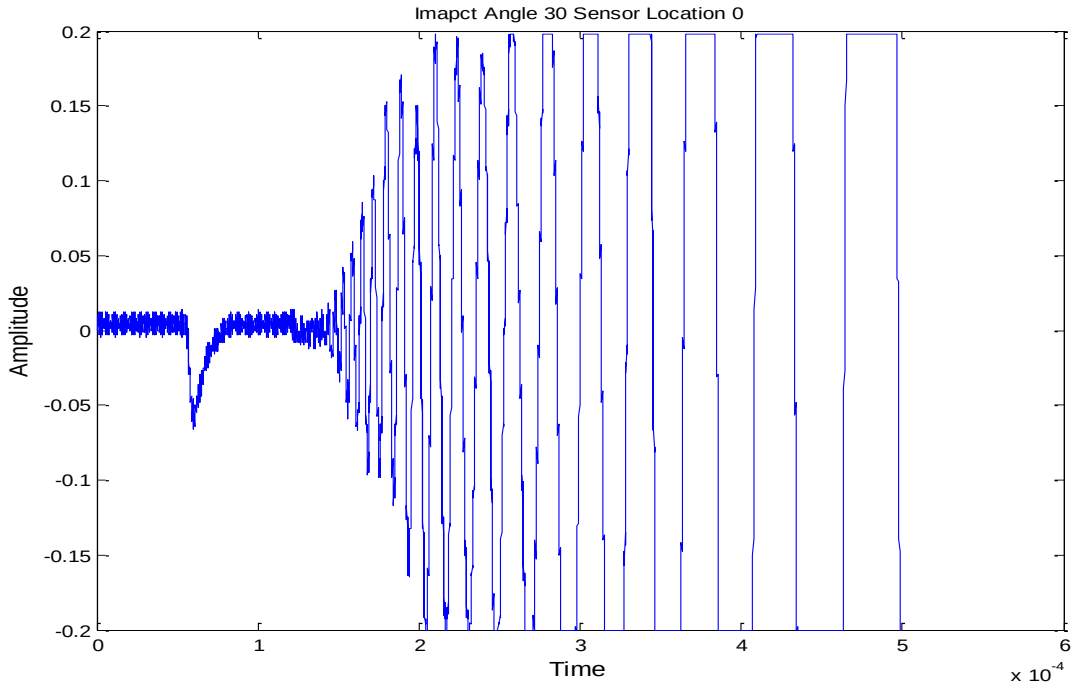

Waveforms captured by the sensors at 45 degrees and 0 degree for a 30 degree impact by a 20 mm diameter ball